ANTIBODY GLYCOENGINEERING FOR DRUG DELIVERY APPLICATIONS

A Thesis

SUBMITTED TO THE FACULTY OF

UNIVERSITY OF MINNESOTA

BY

Drishti Navin Sehgal

IN PARTIAL FULFILLMENT OF THE REQUIREMENTS

FOR THE DEGREE OF

DOCTOR OF PHILOSOPHY

Jayanth Panyam

Advisor

December 2019

Acknowledgements

The past five years were a tremendous learning experience. Several people have contributed selflessly to my growth, and I take this opportunity to thank them.

I cannot thank my adviser, Dr. Jayanth Panyam, enough for his guidance and support during my graduate studies. His enthusiasm towards science was a constant source of inspiration for me. I have yet to meet as patient and understanding person as him.

My parents and sister Isha for their constant love and support. It is my parents who deserve the credit for my academic endeavors. This would have been a much harder journey without their daily words of encouragement. Thank you Piyush, for always believing in me and adding flavor to my boring life. I would have been much crankier and grouchier person by now, if I had not met you.

I am also extremely thankful to the Department of Pharmaceutics. Specifically, Katie James and Amanda Hokanson, for being my magical genies and making my life a lot easier. Dr. William Elmquist, Dr. Tim Wiedmann and Dr. Ben Hackel for being in my thesis committee and their valuable time. I would also like to thank Dr Swayam Prabha for always guiding me through all my challenges.

I would like to thank past and present lab members. Specifically, Ameya, Stephan, Hynjoon and Tanmoy for teaching me everything patiently. Buddhadev, for always being helpful and guiding me in right direction. Manan, thank you for your contribution in completing my thesis projects.

I have had the opportunity to work with several of Dr. Panyam's collaborators. This has enriched my PhD experience. I would particularly thank Dr Thomas Griffith for greeting me with warm welcome and allowing me to use his recourses. I would also like

to thank Tammy for helping me with all my experiments in Griffith Lab. I also appreciate the technical assistance offered by Brenda Koniar, Jane Diamond, Jim Fisher, Guillermo Marques and the flow cytometry core.

Finally, I would like to thank my friends and family for always showering me with their love and support. You all always reminded me to have fun outside lab.

Dedication

This thesis is dedicated to my parents for their unconditional love and support.

Abstract

Monoclonal antibodies (mAbs) are frontline drugs for the treatment of many diseases including cancer [1] and rheumatoid arthritis [2]. In addition to their natural role as neutralizers of pathogens and toxins as well as in the recruitment of immune elements (complement, improving phagocytosis, antibody dependent cytotoxicity), they can be used as carriers for tumor-targeted delivery of therapeutic and diagnostic agents [3]. However, conjugation of drug or drug-encapsulated nanoparticles to antibodies can often result in reduced affinity of the antibody towards the target antigen.

The overall objective of this thesis is to advance a new antibody glycoengineering technology that will allow for facile synthesis of antibody-based drug delivery systems. Most therapeutic mAbs are of the IgG class, which contains a glycosylation site in the Fc region at position 297 [4]. In chapter 2, we investigated a glycoengineering strategy that enables the introduction of artificial azide groups at this glycosylation site without affecting their antigen affinity. This is based on the observation that glycosyltransferases present in mammalian cells can incorporate non-natural sugars (e.g., azido mannose) at glycosylation sites on an IgG molecule during the post translational modification. The azide groups in these artificial sugars are then available to react with alkynes through copper-catalyzed 'click' chemistry or with strained alkynes such as dibenzyl cyclooctyne (DBCO) allowing for biorthogonal, copper-free 'click' chemistry. Because the sugars are added reproducibly and at a site that does not affect antigen binding, the glycoengineering technology would overcome problems associated with traditional conjugation strategies. Using this approach, azide groups were introduced in anti-CD133 and anti-perlecan (AM6) antibodies. Further,

the azide groups were available to react with various DBCO conjugates including fluorophores, drug molecules and nanoparticles. Importantly, the addition of artificial sugar and subsequent azide-alkyne reaction did not affect the affinity of the antibody for the target antigen.

Antibody–drug conjugates (ADCs) have emerged as the next generation anticancer therapeutic agents. In chapter 3, glycoengineered AM6 antibody was used to generate an ADC with monomethyl auristatin E (MMAE) as the cytotoxic drug. The glycoengineering approach resulted in an ADC with a DAR of 2-3 drug molecules per antibody. The AM6-MMAE conjugate demonstrated enhanced cell kill in vitro and significantly improved anticancer efficacy in vivo compared to free MMAE.

Similarly, in chapter 4, glycoengineered AM6 antibody was used to generate antibody conjugated polymeric nanoparticles loaded with paclitaxel. These perlecan-targeted nanoparticles showed enhanced antitumor efficacy in vitro and in vivo in TNBC tumor models. Similarly, antibody conjugated nanoparticles showed enhanced antitumor efficacy in vitro and complete tumor growth inhibition in vivo in a non-muscle invasive bladder cancer model. We expect that this glycoengineering strategy will prove to be a unique platform technology that will have a significant impact on antibody-based therapeutics.

Table of Contents

List of Figures

List of Abbreviation

ADC	Antibody drug conjugate
ADCC	Antibody-dependent cellular cytotoxicity
ADCP	Antibody-dependent cellular phagocytosis
ANOVA	Analysis of variance
BSA	Bovine serum albumin
CD	Cluster of differentiation
CDC	Complement-dependent cytotoxicity
CDR	Complementarity determining region
C_{H1}, C_{H3}, C_{H3}	Heavy chain constant domains 1, 2 and 3, respectively
C_L	Light chain constant domain
DI water	De-ionized water
EGF	Epidermal growth factor
EGFR	Epidermal growth factor receptor
EPR	Enhanced permeability and retention
Fab	Fragment antigen binding
FACS	Fluorescence activated cell sorting
FBS	Fetal bovine serum
Fc	Fragment crystalline
FcGR	Fcg receptor
FcRn	Neonatal Fc receptor
IgA	Immunoglobulin A

IgD	Immunoglobulin D
IgE	Immunoglobulin E
IgG	Immunoglobulin G
IgM	Immunoglobulin M
IHC	Immunohistochemistry
IV	Intravenous
MEM	Minimum essential medium
NK Cell	Natural killer cell
PLA-PEG	Poly lactic acid – poly ethylene glycol
PLGA	Poly(D,L-lactide-co-glycolide)
RBC	Red blood cells
RPMI	Roswell park memorial institute
SC	Subcutaneous
scFv	Single chain fragment variable
VL	Light chain variable domain
TNBC	Triple negative breast cancer

Chapter 1: Introduction

1.1. Introduction to Monoclonal Antibodies

The hypothesis that the immune system recognizes cancer cells as foreign has gained much traction in the past two decades [5]. In fact, a large fraction of the newer class of anti-cancer therapeutics are largely focused on modulating the immune system to improve recognition of cancer cells [6]. Following suit, antibodies have become a major focus for the development of new cancer therapeutics [7].

Over the past three decades, there has been a consistent increase in the number of monoclonal antibody products that have been approved [8]. Their stability, minimal toxicity (relative to cytotoxic drugs) and pharmacokinetic properties are some of the desirable attributes for pharmaceutical development [1]. The key properties of antibodies that enable their widespread application as immuno-therapeutics include their specificity and high affinity for the target antigen [1,9]. In addition, their clinical success is a definite motivation for further investment, considering that of the 41 novel drugs that have been approved by the USFDA, 16 are some form of an antibody (as of December 9th, 2019; data accessed from US-FDA official website).

1.2. Development of Monoclonal Antibodies

The innate arm of the immune system is effective in defending the body against pathogens that are 'typical' in nature or those that have classical molecular patterns. However, in order to fight a wide range of insults, the immune system also consists of an adaptive arm. B cells, a part of the adaptive immune system, recognize antigens through

the B cell receptor [10,11]. Upon Helper T cell mediated stimulation, B cells secrete antibodies that are able to specifically bind to these foreign antigens. Circulating antibodies, also

termed as immunoglobulins (IgGs) [11,12], are then able to eliminate antigens by two potential mechanisms: one involves directly binding to and neutralizing the antigen, and the other is to recruit innate immune components (complement proteins, NK cells, macrophages, and dendritic cells) that are able to eliminate the antigen from the system [10–12].Thus, the idea behind the development of exogenous monoclonal antibodies is to enable the human body to recognize pathogens or tumor antigens that it may have missed.

B cells can develop antibodies to virtually any type of antigen, including pathogens as well as small molecules [13]. They secrete antibodies that bind to a vast variety of antigens. On average, a human has the ability to produce greater than 10^8 - 10^{10} different types of specific antibodies due to specialized processes of the immune system [14]. The hybridoma technology, developed by Kohler and Milstein, was an attempt to utilize these 'specialized processes' for the development of clinical therapeutics [15]. It involved immunizing animals (often mice or rabbits) repeatedly with an antigen of interest causing B cells to secrete antibodies specific to that antigen. Along with several following downstream processes, this technology provided researchers with the much-needed capability to artificially develop antibodies against specifically selected antigens. In addition, it also provided a means to produce large quantities of antibodies *in vitro* [16,17]. Kohler and Milstein were awarded the 1994 Nobel

Prize in Medicine/Physiology for their work in the development of hybridoma technology [18].However, due to their non-human origin, hybridoma antibodies have had limited clinical success[19]. Mouse antibodies suffer from significant immunogenicity and are unable to interact with other immune components when administered in humans[20]. These issues were addressed by the development of chimeric and humanized antibodies from hybridoma clones, that replaced portions of the mouse antibody sequence with human antibody sequences [21,22]. This led to the development of several tumor-targeted antibodies that have been clinically successful. The first chimeric monoclonal antibody approved for cancer treatment was Rituximab (Rituxanâ) [23], an anti- human CD20 binding antibody with mouse and human sequences combined[13].

Twenty four years after Kohler and Milstein received the Nobel prize for hybridoma work, Sir Gregory Winter and George Smith were awarded the Nobel Prize for phage display [24]. The technology has allowed scientists to develop fully-human antibodies against virtually any antigen of interest, *in vitro*. This method uses large, diverse libraries of bacteriophage (bacterial viruses) displaying antibody fragments on their surface for *in vitro* high-throughput screening of antibody fragments against the desired peptide/antigen. Sequential enrichment of antibody fragments that display specificity for the given target eventually leads to a manageable number of candidates that can be reformatted into fully human IgGs using modern molecular biology techniques. Adalimumab (Humiraâ) [25], the first approved monoclonal antibody developed using phage display, is used for the treatment of various auto-immune

disorders [26]. It was approved in the US in 2002 and has since topped the list of highest selling drugs in the US [27]. Phage display was a significant advancement over the hybridoma technology, that despite its success, suffered from several limitations such as being labor and time intensive. In addition to being an immensely useful tool in the development of antibodies, phage display can also be utilized for the discovery of novel targets [28]. Analogous to the use of tumor gene expression profiles to evaluate the presence of mutations or anomalous overexpression, phage display can be used to identify new targets in their native, physiological format.

1.3. Antibody Structure and Classification

Antibodies can be classified into five different sub-classes based upon their structure. These include IgA, IgD, IgM, IgG and IgE [9]. Each sub-class has its own unique but complementary immune functions. The most abundant type of antibody in blood is IgG. It comprises 10-20% of the total plasma protein component and about 80-90% of the total plasma antibody component [9,29]. IgG is also the most extensively studied class of antibodies, representing more than 70% of all antibody based therapeutics [30]. From here on, any reference to antibodies (unless otherwise specified) will be made with respect to IgG antibodies. Each IgG molecule is a Y-shaped molecule (~150 kDa) consisting of four polypeptide chains, two identical heavy chains (~50 kDa each) and two identical light chains (~25 kDa each) [9]. Two disulfide bonds link the two heavy chains together and one disulfide bond, each, links the two heavy chain-light chain pairs together (Figure 1.1) [11]. In humans, there are five types of heavy

chains (α, μ, γ, ε and δ) that determine the antibody classification of IgA, IgM, IgG, IgE and IgD, respectively. There are also two types of light chains classified as κ and λ [9].

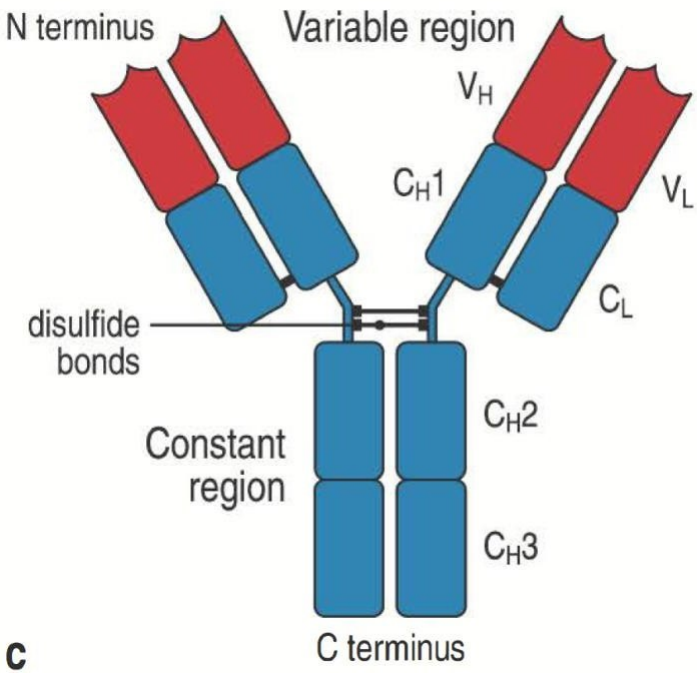

Figure 1.1: Structure of an IgG antibody. Image modified from Janeway's Immunobiology

Each light chain can be further sub-divided into the constant (C) domain and the variable (V) domain i.e., C_L and V_L, respectively. The heavy chain can be sub-divided into three constant domains and one variable domain i.e. C_{H1}, C_{H2}, C_{H3} and V_H, as well as an additional hinge region between C_{H1} and C_{H2} (Figure 1.1). Antibodies of classes other than IgG also have the same basic framework of heavy and light chains; however, variability in the heavy chain allows for different effector functions for different sub- classes.

Regions of an antibody can be grouped together structurally or functionally. Structurally, V_L and V_H are grouped together to form the variable region that is responsible for the expansive diversity observed in antigen binding [11]. More specifically, within each variable domain (V_H and V_L) are found three hypervariable regions or complementarity determining regions (CDRs) that allow for the highly diverse antigen binding [31]. Thus, each antibody can have six unique CDRs. Polypeptide chains outside the CDRs but within the variable domains are termed as 'framework'. On the other hand, the C_L and C_H regions are grouped together to form the constant region that varies only subtly, allowing for different effector functions.

Functionally, V_L, C_L and V_H, C_{H1} together form the 'fragment antigen binding' (Fab) [11]. The presence of two Fab arms makes antibodies bivalent in nature i.e., they simultaneously bind to two antigen molecules, thus increasing the total strength of interaction through avidity [9]. On the other end, C_{H2} x2 and C_{H3} x2 together form the 'fragment crystalline' (Fc) portion of the antibody or the 'stem' of the antibody [11].

Thus, an antibody can be thought to have two primary functions; the first, to bind to a unique target antigen, and the second, to bind to different components of the immune system. As the name suggests, the Fab arm of an antibody binds to the target antigen, whereas the Fc region binds to different immune components and determines its effector function. The Fc region is also a critical determinant of antibody pharmacokinetics, a property that is significantly different from that of traditional small molecule compounds. It is important to note here that, even though the Fab domains make antibodies unique and desirable for pharmaceutical development, the

Fc domains are critical to antibody function and influence the outcome of therapeutic antibodies.

Therapeutic mAbs and derivatives have an asparagine (Asn)-X-Ser/Thr (where X is any amino acid except a Pro) consensus sequence for N-glycosylation at the position Asn297 in the heavy chain of the CH2 constant domain [32]. Some therapeutic mAbs also bear additional glycosylation in the Fab domain such as at Asn88 of the VH region in the case of cetuximab[7]. In addition, some of the Fc-fusion partner molecules such as etanercept and B cell-activating factor receptor 3 (BR3)–Fc also possess O-linked glycans [33,34]. Alteration of glycan compositions and structures can cause conformational changes of the Fc domain, which could change binding affinity to Fc receptors, resulting in changes to immune effector functions [35,36]. Fc effector functions include complement-dependent cytotoxicity (CDC), antibody-dependent cell-mediated cytotoxicity (ADCC), and antibody-dependent cell-mediated phagocytosis (ADCP) [35]. All three effector functions are triggered by the formation of immune complexes, which then recruit complement proteins and/or effector cells [32].

1.4 IgG N-glycan structure and biosynthesis

Unlike other serum proteins, the N-linked glycans of human IgGs are typically biantennary complex structures (Figure 1.2). A conserved core structure is composed of two N- acetylglucosamine (GlcNAc), three mannose, and two GlcNAc residues that are b-1,2 linked to a-6 mannose and a-3 mannose, forming two antennae. Additional monosaccharides extended from the core may be present. Depending on the host

glycosylation machinery, additional fucose (Fuc), galactose (Gal), bisecting GlcNAc, and sialic acid including N-acetylneuraminic acid (NANA) or N-glycolylneuraminic acid (NGNA) residues, may be added to the core. Glycans present considerable heterogeneity with more than several hundred possible glycoforms because of the random pairing of heavy-chain glycans with different structures [7,37]. The a-1,6 arm of the biantennary glycan extends along the hydrophobic face of the CH2 amino acid backbone where the polar nature of the carbohydrate protects the underlying hydrophobic polypeptide. The a-1,3 arm of the glycan extends toward the interstitial space formed by the CH2–CH3 dimer. The glycans on opposite Asn297 residues of each heavy chain interact and maintain the conformation of the Fc domain. As such, changes in Fc glycosylation can alter the Fc conformation and subsequent binding to Fc receptors [38].

Antibody N-linked glycan biosynthesis follows the same process as for other glycoproteins [39–41]. A preassembled Glc3Man9GlcNAc2 oligosaccharide is transferred to Asn297 of the IgG heavy chain by an oligosaccharyl transferase complex in the endoplasmic reticulum, followed by glycosidase-mediated sequential removal of three Glc residues and a mannose residue to form Man8GlcNAc2. After transition to the cis-Golgi apparatus, three additional mannoses are trimmed by mannosidase to form a Man5GlcNAc2 oligosaccharide. Once in the medial golgi, the N-acetylglucosaminyltransferase–I (GnT- I) enzyme mediates the transfer of GlcNAc from UDPGlcNAc to the O-2 position of the terminal mannose residue in the a1 → 3 branch of the Man5GlcNAc2 oligosaccharide. Subsequently, removal of two more

mannose residues from the a1→6 branch gives rise to a GlcNAcMan3GlcNAc2 oligosaccharide. Before translocating to the trans-Golgi, N-acetylglucosaminyltransferase–II (GnT-II) mediates the transfer of an additional GlcNAc to the newly generated terminal mannose residue at the O-2 position in the a1→6 branch to form the conserved biantennary core structure GlcNAc2Man3GlcNAc2 [39]. In the trans-Golgi, the addition of Gal, bisecting GlcNAc, sialic acid (either NANA or NGNA) and core Fuc residues occurs via enzymatic addition by specific transferases using nucleotide-charged monosaccharide donors. Figure 1.3 summarizes the major steps of N-linked glycan biosynthesis. Specific glycosylation patterns are associated with different effector functions. For instance, high mannose variants (Man5/8/9) would also lack core Fuc, resulting in higher binding affinity to FcRIIIa and enhanced ADCC activity.

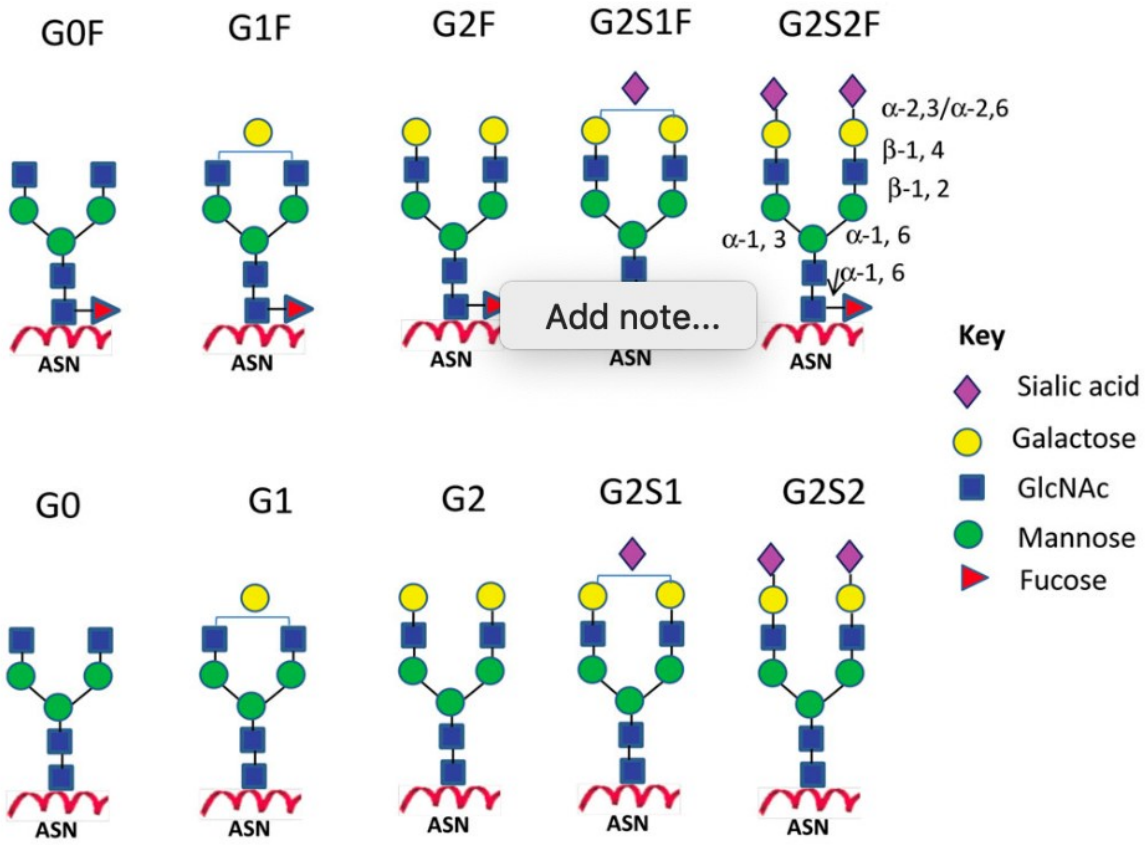

Figure 1.2: Major N-linked glycoforms of mAb therapeutics [32].

.

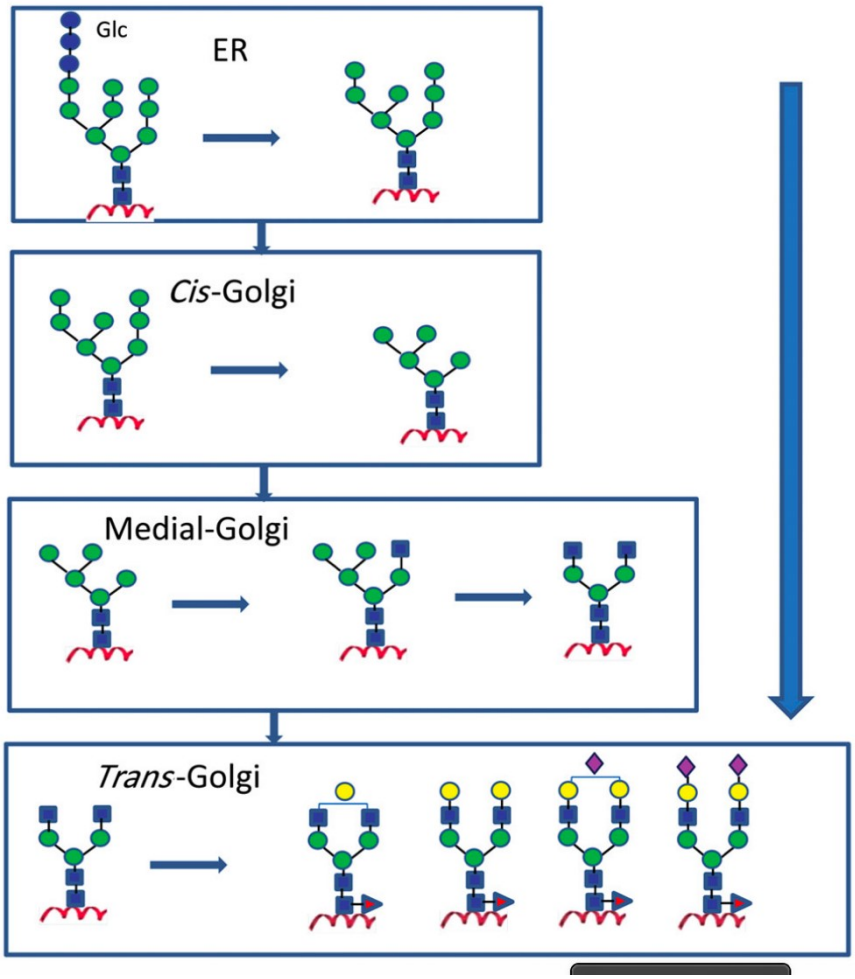

Figure 1.3: Antibody N-linked glycan biosynthesis pathways. Schematic presentation is based on the work of Kornfeld and Kornfeld [39].

1.5 Click chemistry

Click chemistry is a method for attaching a probe or substrate to a specific biomolecule, a process called bioconjugation. A fluorophore or reporter molecule can be attached via click chemistry and this has made it a powerful tool for identifying, locating, and characterizing both old and new biomolecules. The classic [42] click reaction is formation of a 5-membered heteroatom atom ring by azide and alkyne in presence of copper: a Cu(I)-catalyzed azide alkyne cycloaddition (CuAAC).

However, the use of the copper-catalyzed azide–alkyne cycloaddition (CuAAC) was severely compromised in the context of biological matter, due to the toxicity of the inevitable copper(I)species to living cells and organisms. With the clever insight by researchers at the University of California, Berkeley [43] who came up with strain-promoted azide alkyne cycloaddition (SPAAC) of cyclooctynes with azides is a highly versatile copper-free version of the popular click reaction [4445]. This is an efficient and clean bioconjugation tool and the usefulness of cyclooctyne–azide cycloaddition is now adopted in a wide range of fields of chemical science and beyond. Its ease of operation, broad solvent compatibility, 100 % atom efficiency, and the high stability of the resulting triazole product, just to name a few aspects, have catapulted this so-called strainpromoted azide–alkyne cycloaddition (SPAAC) right into the top-shelf of the toolbox of chemical biologists, material scientists, biotechnologists, medicinal chemists, and more.

1.6. Antibodies as Therapeutics

With the advent of advanced hybridoma techniques and phage display, antibodies are being investigated for several different applications in research and in the clinic. In research, antibodies have become an indispensable reagent for various experimental techniques. However, for the purpose of this thesis, clinical application of antibodies is the focus. Antibodies in the clinic have been utilized in versatile applications including, but not limited to, antibody-drug conjugates, diagnostic agents, targeting ligands and as therapeutics themselves. Here we will focus on the two classes

that have been used as therapeutics for cancer therapy, antibody-drug conjugates and antibody conjugated nanoparticles.

1.6.1. Antibody Drug Conjugates (ADCs)

ADCs are a special class of therapeutics that have gained significant attention in the past decade. The idea behind ADCs is to specifically deliver cytotoxic drugs to the tumor by leveraging a key property of antibodies i.e. specificity, and in turn sparing normal cells of toxicity. ADCs consist of a monoclonal antibody conjugated, via a linker, to an extremely potent drug.

Currently, there are six FDA approved ADCs, including brentuximab vedotin (AdcetrisÒ) [46] for the treatment of CD30 positive Hodgkin's lymphoma, ado-trastuzumab emtansine (KadcyclaÒ) [47] for the treatment of HER2 positive breast cancer, gemtuzumab ozogamicin (MylotargÒ) [48] for the treatment of CD33 positive acute myeloid leukemia, inotuzumab ozogamicin (BesponsaÒ) [49] for the treatment of CD22 positive acute lymphoblastic leukemia, moxetumomab pasudotox (LumoxitiÒ) [50] for relapsed or refractory haircell leukemia (HCL) and polatuzumab vendotinpiiq (PolivyÒ) [51] for diffused large B cell lymphoma (DLBCL).

Mechanism of action of ADC: When designing an ideal ADC, it is essential to understand the mechanism of action in order to identify the desired features of each of its three components. An ideal ADC is one that retains the selectivity of a mAb while still being able to release the cytotoxic drug in quantities large enough to kill tumors

cells. Each of the steps involved in the mechanism of action is associated with unique challenges that complicate the design of ADCs [52]. These are illustrated in Figure 1.4. ADCs are administered intravenously in order to prevent the mAb from being destroyed by gastric acids and proteolytic enzymes. The mAb component of the ADC enables it to circulate in the bloodstream until it finds and binds to tumor cell -specific surface antigens or tumor microenvironment-associated targets. In the interest of preventing unwarranted release of the cytotoxin and maximizing drug delivery to cancer cells, an ideal linker would not only have to be stable in the bloodstream but also capable of releasing the active form of the

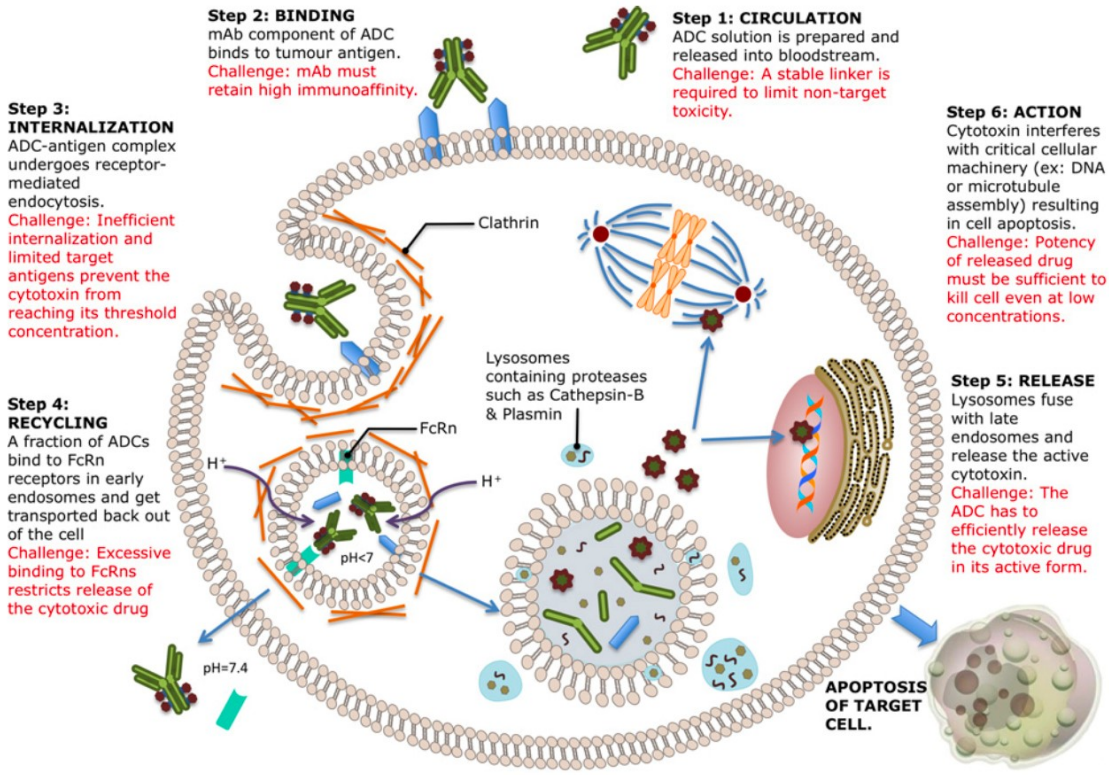

Figure 1.4: Mechanism of action of ADC[53]

cytotoxic drug when required [54]. Once the mAb component of the ADC is bound to its target antigen, the ADC–antigen complex should theoretically be internalized via receptor-mediated endocytosis. The internalization process finishes with the formation of a clathrin coated early endosome containing the ADC–antigen complex [55]. An influx of H+ ions into the endosome results in an acidic environment that facilitates the interaction between the mAb component of a fraction of ADCs and human neonatal Fc receptors (FcRns). The bound ADCs are transported outside the cell, where the physiological pH of 7.4 enables the release of the ADC from the FcRn [56]. This mechanism acts as a buffer for preventing the death of healthy cells in the case of ADC mis-delivery. Excessive binding of ADCs to tumor cell FcRns might however restrict the release of the cytotoxic drug and prevent the ADC from taking effect [57]. FcRn expression is primarily within the endosomes of endothelial cells. ADCs that remain in the endosome without binding to FcRn receptors form the late endosome. These subsequently undergo lysosomal degradation, allowing the release of the cytotoxic drug into the cytoplasm. At this stage, it is crucial to ensure that a sufficient (i.e. threshold) concentration of the drug is present within the cancer cell for its destruction to be guaranteed. This is however complicated in practice by the facts that cell-surface antigens are often quite limited and the process of internalization rather inefficient [58]. Assuming all the steps involved in the mechanism of ADC action have an efficiency of 50%, only 1%–2% of the administered drug will reach tumor cells [59]. This makes the choice of cytotoxin particularly important, as it is required to be highly efficacious at very low concentrations. Drugs that are usually unsuitable for normal chemotherapy (due to excessive toxicity) are therefore a necessary component of

ADCs. Different classes of cytotoxic drugs result in cell death using various mechanisms [53]. The common element between all the classes is interference with critical cell functioning and, as a consequence, either direct killing of the cell or induction of apoptosis. As targeted cancer cells die, there is potential for the active cytotoxic drug to kill neighboring tumor cells and the supporting stromal tissue. The design of ADCs with respect to the choice of target, mAb, linker and cytotoxin are all very important determinants of whether or not the threshold concentration of the cytotoxic drug is reached within the tumor cell. These factors therefore determine the overall success of an ADC.

Key Components of ADC: ADCs have three components: antibody, linker and drug. The antibody should be specific for a cell surface target molecule that is selectively expressed on cancer cells, or overexpressed on cancer cells relative to normal cells [60]. The payload of an ADC must be highly cytotoxic so that it can kill tumor cells at the intracellular concentrations achievable following distribution of the ADC into tumor tissue, and because only a limited number of drug molecules can be linked to an antibody molecule (typically, an average of 3–4 per antibody) without severely compromising its biophysical and pharmacokinetic properties [60–62]. Indeed, the breakthrough in ADC research that eventually led to the creation of approved and marketed products came with the realization that the cytotoxic agents suitable for ADC approaches need to have potency in the picomolar range to be able to be delivered in sufficient quantity to enough cancer cells to effect a therapeutic benefit [60–62]. The cytotoxic compounds used in approved and marketed ADCs are derivatives of calicheamicin, a class of highly cytotoxic enediyne antibiotics which kill cells by

causing DNA double-strand breaks [60,63], and derivatives of the potent antimitotic microtubule-

disrupting agents, dolastatin 10 (auristatins) [61,64] and maytansine [62,65,66]. The third vital component of an ADC is the linker that forms a chemical connection between the payload and the antibody. The linker should be sufficiently stable in circulation to allow the payload to remain attached to the antibody while in circulation as it distributes into tissues (including solid tumor tissue), yet should allow efficient release of an active cell-killing agent once the ADC is taken up into the cancer cells [60]. Linkers can be characterized as either cleavable, where a chemical bond (or bonds) between the payload and the attachment site on the antibody (usually an amino acid) can be cleaved intracellularly [67,68], or as non-cleavable, where the final active metabolite released within the cell includes the payload and all elements of the linker still attached to an amino acid residue of the antibody, typically a lysine or a cysteine residue, following complete proteolytic degradation of the ADC within the lysosome of the cell [69–72].

The design goal for an ADC is to harness the potent tumor cell-killing action of the payload, while retaining the favorable in vivo pharmacokinetic and biodistribution properties of the immunoglobulin, as well as any intrinsic biologic or immunologic activity it may have [60,62,69–72]. Much of the selection of the optimal antibody, the ideal linker–payload chemistry, and the optimal number of payload molecules linked per antibody molecule, are determined empirically, with a focus on maximizing the therapeutic index of the ADC [60,72].

1.6.2. Antibody conjugated nanoparticles

Nanomedicine has gained significant importance in cancer therapy over the past few years. The primary advantage of nanoparticles is their size range (1 to 500 nm) due to which they are internalized into cells better than larger sized delivery systems such as microparticles [73]. This is essential for chemotherapeutic drugs such as paclitaxel that act intracellularly. The surface properties of nanoparticles can be modified to be hydrophobic or hydrophilic depending upon the requirement. Further, a drug loaded in nanoparticles remains protected for longer, and nanoparticles can be formulated to act as a controlled release reservoir for the drug. Nanoparticles have also been engineered for targeted drug delivery to avoid toxicity and improve efficacy [74]. Nanoparticles also have a unique passive targeting feature in case of cancer therapy.

In normal tissues, the blood vessels are lined by tightly packed endothelial cells that are highly selective in terms of what moves out of the lumen into the interstitial fluid. As opposed to this, in case of tumors, the vasculature is leaky and pores between endothelial cells are abnormally large [75]. This is due to rapid and incomplete development of the tumor vasculature. Additionally, the tumor vasculature has a missing layer of pericytes surrounding the vessels. This uniquely leaky vasculature of the tumor allows nanoparticles to preferentially “leak” out of the blood vessels and move into the tumor interstitial fluid. This would not be possible in case of other organs due to the tight endothelial junctions, liver being the exception.

Under normal conditions, fluid draining from the blood vessels into tissue is cleared via the lymphatic system. However, tumors lack an efficient lymphatic system, as a result of which, there is elevated interstitial fluid pressure (IFP) [76]. Thus, the nanoparticles move into the tumor relatively easily and are unable to move out. This phenomenon of preferential uptake of nanoparticles followed by prolonged retention in the tumor is termed as the "Enhanced Permeability and Retention" effect or the EPR effect [77].

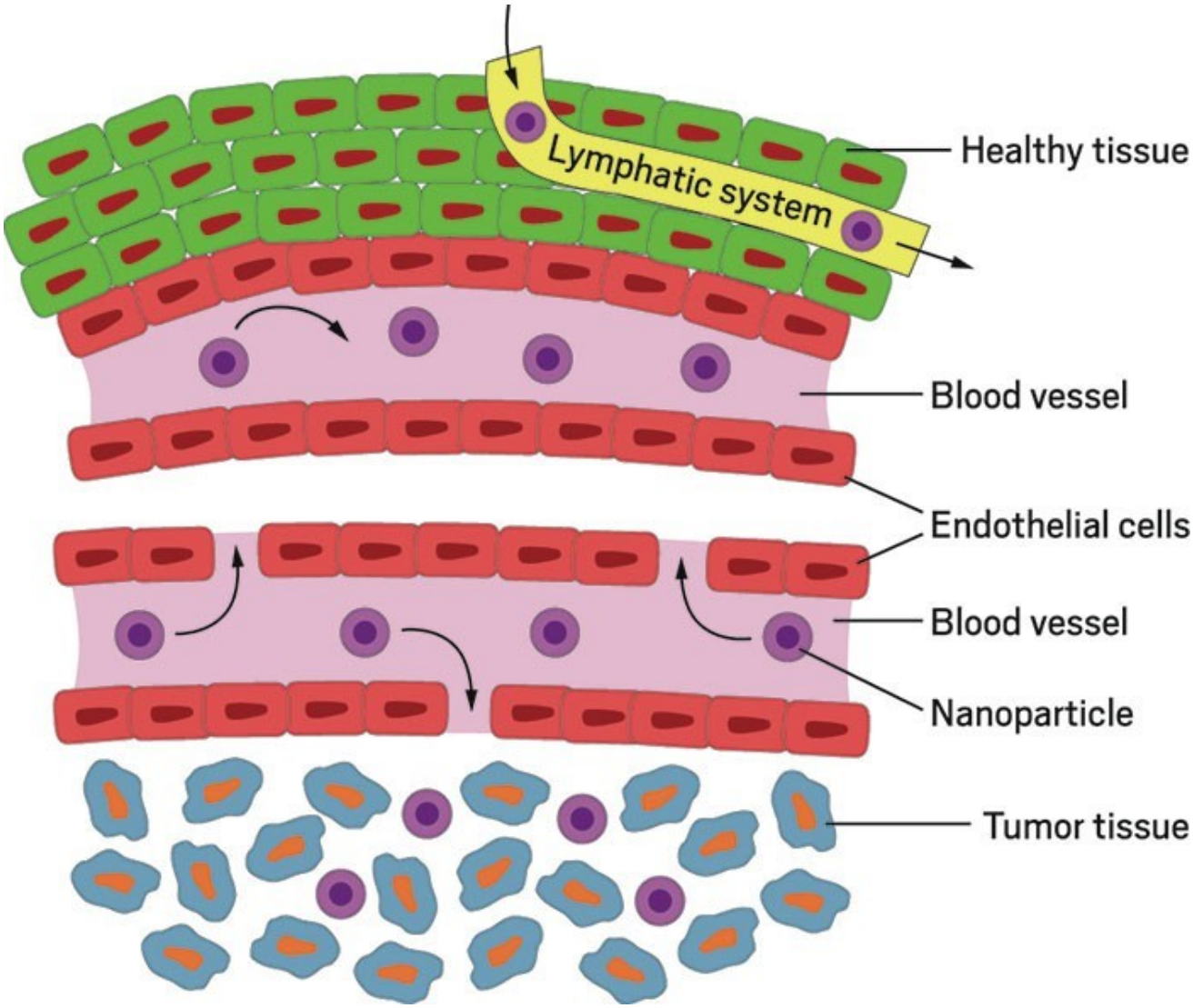

Figure 1.5 Enhanced permeation and retention effect[78]

Although the EPR effect has been of the main driving force for the development of cancer nanotherapeutics, it is important to recognize that the EPR effect is not a universal phenomenon.

Not all tumor vessels are leaky to the same extent, not all pores are of uniform size, and thus, not all tumors exhibit the EPR effect.

An extension of the EPR effect is active targeting. Actively targeted drug delivery involves the use of specific ligands that are able to recognize antigens or proteins that are overexpressed by the tumor. The ligands used for active targeting generally involve proteins, the most popular being antibodies and their fragments. In vivo stability, availability of different forms of antibodies (scFv, Fab fragment, dimers, whole antibody), and the availability of a myriad of techniques for antibody engineering makes them highly amenable for use in targeted drug delivery. Active targeting enables nanoparticles to "actively" bind to the cell surface and undergo receptor mediated internalization [74]. Not only does active targeting provide the carrier with additional means for endocytosis, but also a target to "hold on" to in the tumor, resulting in improved retention. Recent reports have pointed out that the main advantage of actively targeted nanoparticles is the improved internalization of nanoparticles, however the overall biodistribution remains unchanged [79,80]. Targeted drug delivery (active or passive) has the potential to reduce the toxicity associated with the drug and improve its overall efficacy.

Poly(DL-lactide-co-glycolide) (PLGA), an FDA approved polymer, has been one of the most commonly employed polymers in controlled release formulations and

tissue engineering applications due its safety, acceptable toxicity profile, biocompatibility and biodegradability [81]. PLGA is degraded in vivo by hydrolysis into biologically compatible lactic acid and glycolic acid, both of which are eliminated from the body via the tricarboxylic acid (TCA) cycle. Drug release from PLGA matrix takes place initially by simple diffusion, followed by a combination of drug diffusion and polymer degradation. The rate of drug release from PLGA matrices can be customized by varying the lactide to glycolide ratio and the molecular weight of the polymer [82]. Additionally, PLGA nanoparticles have been observed to escape endo-lysosomal degradation via a pH dependent charge reversal, prolonging their half-life within the cell [83]. Based on these desirable properties, we used PLGA to formulate nanoparticles in our studies.

Despite its several advantages, PLGA still faces the most common pharmacokinetic problem observed with nanoparticles – rapid clearance by the mononuclear phagocytic system (MPS) [84]. Once nanoparticles are injected into the bloodstream, they are almost instantly covered by opsonins that tag them as "foreign" for phagocytosis by macrophages. This results in rapid clearance of nanoparticles from the bloodstream, preventing them from reaching the site of action. In order to overcome this issue, multiple solutions have been tried, but by far the most successful and most popular is termed as 'PEGylation'. PEGylation involves the introduction of poly(ethylene glycol) or PEG chains on the surface of nanoparticles. Presence of the PEG layer forms a hydrophilic barrier, reducing adsorption of opsonins. This allows nanoparticles to remain "hidden" from the MPS, significantly extending their circulation half-life [85].

Our lab uses the emulsion-solvent evaporation process for nanoparticles synthesis. In brief, this involves formulation of an oil-in-water emulsion with the polymer dissolved in the oil phase (organic solvent), followed by evaporation of the oil phase to form solid nanoparticles. An earlier publication from our lab describes the introduction of surface functional groups on nanoparticles by Interfacial Activity Assisted Surface Functionalization (IAASF) [86]. This particular method is applicable to the solvent-emulsion evaporation technique of nanoparticle formulation. After the oil-in-water emulsion is formed, if a diblock co-polymer is introduced into the emulsion, its hydrophobic portion will align within the oil phase while the hydrophilic portion will align in the water phase. This expected orientation can be utilized to our advantage by the introduction of the required functional group on the hydrophilic portion of the polymer that will align outwards. We used IAASF for the introduction of PEG with terminal DBCO groups on the nanoparticle surface. These DBCO functional groups were then used to functionalize nanoparticles with glycoengineered antibodies via copper-free click chemistry.

1.7. Current approaches in antibody conjugation and challenges

As in the previous section we have seen that therapeutic activity of an antibody can also be improved by conjugating it to a cytotoxic payload directly or to a moiety loaded with cytotoxic payload. There are many chemical, enzymatic and chemoenzymatic methods used to modify the antibody for conjugation.

Interchain disulfide bridges and surface-exposed lysines are the most currently used residues on the antibody for conjugation, respectively (>50 *vs*. >30%) [87]. Theoretically, the linkage of cytotoxic payloads to the surface-exposed lysine of mAb occurs after reduction of ∼40 lysine residues on both heavy and light chain of mAb and it results in 0–8 cytotoxic payload linkages per antibody and heterogeneity with about one million different antibody conjugated species [60,67,88]. Cysteine conjugation occurs after reduction of four interchain disulfide bonds and results in eight exposed sulfhydryl groups. Linking payload per antibody can differ from zero to 8 molecules, generating a heterogeneous population of antibody conjugated species (Greater than one hundred different species). It is possible to reduce just two of four interchain mAb's disulfide bonds of cysteine residues through carefully mild reduction conditions, as interchain disulfide bridges are

more prone to reduction than intrachain disulfide bridges [17,31,89–91]. However, such mild reduction

is not easily possible in practice and a diverse number of cysteines may be reduced (0–4), resulting in a heterogeneous mixture [87,88].

Due to low stability and safety properties of the pharmaceutical products with heterogeneous contents, they are complex to be accurately predicted in terms of efficacy or therapeutic window [87,92]. Therefore, improvement of conjugation methods to achieve homogeneous product is very crucial.

Recently, site-specific enzyme-mediated and chemoenzymatic site direct conjugation was established to overcome the above mentioned limitation. This site-specific enzyme-mediated conjugation involves incorporating a thiolated sugar

analogue, 6-thiofucose, to the antibody carbohydrate that introduces new chemically active thiol groups using fucosyltransferase [29,90,91]. Chemoenzymatic site direct conjugation, involves introducing two azide groups at asparagine 297 (Asn-297) residue in antibody constant region (Fc) is linked with cytotoxic payloads using coppermediated click reaction . The azide functional groups are formed in a selective hydrolysis reaction that is mediated by an Endo-beta-N-acetylglucosaminidase (EndoS) chemoenzyme [87,89,91]. However, using copper as a catalyst which is toxic to biological system and post production modification can often result in reduced affinity of the antibody towards the target antigen [92].

1.8. Statement of problem and Specific Aims

Current approaches to antibody-based syntheses involve chemical and enzymatic modifications of pre-formed antibodies [29,90,91]. Such reactions can affect the antigen-affinity and pharmacokinetics of the antibody [92]. The central objective of this thesis is to advance a new antibody glycoengineering technology that will allow for facile synthesis of antibody-based drug delivery systems. The work presented here examines the use of glycoengineered antibodies for the development of antibody drug conjugates and antibody functionalized polymeric nanoparticles. The specific aims of this research were:

1.8.1. Specific Aim 1: Generation of glycoengineered antibodies

Our work in chapter 2 focused on the development of glycoengineered antibodies. We developed glycoengineered anti-perlecan antibody as well as glycoengineered anti-CD133 antibody. These antibodies were characterized and quantified for the presence of azide

groups. Additionally, we compared the antigen binding affinity and tumor accumulation of glycoengineered antibodies.

1.8.2. Specific Aim 2: Synthesis of ADC with glycoengineered anti-perlecan antibody

In chapter 3, we synthesized an ADC using the glycoengineered anti-perlecan antibody developed in chapter 2. We characterized the ADC for drug loading and carried out *in vivo* and *in vitro* studies to determine its therapeutic efficacy in a mouse model of triple negative breast cancer.

1.8.3. Specific Aim 3: Synthesis of antibody conjugated nanoparticles with glycoengineered anti-perlecan antibody

In chapter 4, we synthesized antibody conjugated nanoparticles using the glycoengineered antiperlecan antibody developed in chapter 2. We encapsulated paclitaxel in nanoparticles and surface functionalized the nanoparticles with anti-perlecan antibody to form antibody conjugated nanoparticles. We determine the *in vivo* and *in vitro* therapeutic efficacy of these targeted nanoparticles in mouse models of triple negative breast cancer and non-muscle invasive bladder cancer.

Chapter 2: Development of glycoengineered antibody

2.1 Introduction

Therapeutic mAbs have an asparagine (Asn)-X-Ser/Thr (where X is any amino acid except a Pro) consensus sequence for N-glycosylation at position Asn297 in the constant domain of the heavy chain [7]. The N-linked glycans of human IgGs are typically biantennary complex structures. This conserved core structure is composed of two N-acetylglucosamine (GlcNAc), three mannose, and two GlcNAc residues that are b-1, 2 linked to a-6 mannose and a-3 mannose, forming two antennae. Additional monosaccharides extended from the core may be present. Depending on the host glycosylation machinery, additional fucose (Fuc), galactose (Gal), sialic acid, may be added to the core [32].

Alteration of glycan compositions and structures can cause conformational changes of the Fc domain, which could change binding affinity to Fc receptors, resulting in changes to immune effector functions [36]. Fc effector functions include complement-dependent cytotoxicity (CDC), antibody dependent cell-mediated cytotoxicity (ADCC), and antibody dependent cell-mediated phagocytosis (ADCP) [35,92].

Previous studies have examined the use of N-linked glycans to conjugate therapeutic agents to mAbs. A number of studies have utilized chemoenzymatic technologies to modify the N-glycans [92]. However, such postproduction modification can often result in reduced affinity of the antibody towards target antigen. In this chapter, we report a unique glycoengineering strategy, which allows for substitution of one or all of N-glycan sugars with non-natural sugars containing a reactive group during the production of the antibody. This strategy can then be used for site specific

conjugation of a payload. As this involves metabolic engineering of the antibody in the constant region, target binding affinity is expected to remain unaffected.

We used azide as our reactive group for two main reasons. First, as azide groups are not found in the living system [93], glycoengineering will be the only process through which they will be incorporated in the antibody. Second, the azide groups can be used to easily conjugate a payload with a cyclooctyne group via strain-promoted alkyne-azide cycloaddition also called as copperfree click chemistry [43]. In our studies, we used N-azidoacetylgalactosamine-tetraacylated (Ac4GalNAz) as the non-natural sugar to incorporate azide groups in two different antibodies. The effect of introducing the non-natural sugar on in vitro antigen affinity and in vivo tumor accumulation were determined.

2.2 Methods

2.2.1 Materials

Cell culture supplies were obtained from Invitrogen (Waltham, MA) or Corning (Tewksbury, MA), unless otherwise specified. Fetal bovine serum (FBS) was purchased from Atlanta Biologicals (Flowery Branch, GA). Control isotype IgG (Cat. No. 401114) was purchased from Calbiochem (Billerica, MA). The materials for SDS/PAGE were obtained from Bio-Rad (Hercules, CA). N-azidoacetylgalactosamine-tetraacylated (Ac4GalNAz) sugar, DBCOcarboxyrhodamine dye and DBCO-PEG4-biotin were purchased from Click Chemistry Tools (Scottsdale, AZ). Deionized (DI) water was available through university resources.

2.2.2 Cell Culture

MDA-MB-231-LM2 cells were from Joan Massague Laboraotry and have been previously described as being derived from lung metastasis arising from parental MDA-MB-231 tumors in mice. Cells between passages of 2 and 10 were used for all the studies. Cells were cultured in minimum essential medium (MEM) with 10% v/v fetal bovine serum (FBS) and 1% v/v penicillin/streptomycin in a humidified atmosphere with 5% CO_2. Caco2 cells (a continuous line of heterogeneous human epithelial colorectal adenocarcinoma cells) were obtained from ATCC. Cells were cultured in eagles minimum essential medium (EMEM) with 20% v/v fetal bovine

serum (FBS) and 1% v/v penicillin/streptomycin in a humidified atmosphere with 5% CO_2.

2.2.3 Preparation and purification of glycoengineered antibodies

2.2.3.1 Glycoengineered anti-perlecan antibody

Expi293F Expression System by Life Technologies (Carlsbad, CA) was used for the expression of anti-perlecan antibodies. During the process of production of antibody, 25 μM of Ac4GalNAz sugar was added to the cells with the enhancers a day after transfection and also for subsequent three days. Control antibody was made without the addition of Ac4GalNAz sugar. Seven days after transfection, affinity purification of antibodies was carried out using Protein A Plus (Pierce, Rockford, IL) followed by buffer exchange into tris-buffered saline containing 5mM EDTA. Zeba™ Spin Desalting Columns (87769, Pierce Biotechnology, Rockford, IL) were used for the buffer exchange step. Antibody stocks were stored at -20°C in single use aliquots until use. Once thawed, the samples were placed at 4°C for short-term storage. Quality control evaluation involved resolution via SDS/PAGE for reduced and nonreduced samples and flow cytometry for confirmation of binding affinity.

2.2.3.2 Glycoengineered anti-CD133 antibody

CD133 hybridoma cells [94] were used for the expression of anti-CD133 antibodies. During the process of growing hybridoma cells, when the cells reached 60% confluency, 25μM of Ac4GalNAz sugar was added to the cells for subsequent three days. Control antibody was made without the addition of Ac4GalNAz sugar to

hybridoma cells. After five days, purification of antibody was carried out by using AmiconÒ Ultra-15 Centrifugal filter units, 100KDa (Millipore Sigma, Burlington, MA). Zeba™ Spin Desalting Columns (87769, Pierce Biotechnology, Rockford, IL) were used for the buffer exchange into tris-buffered saline containing 5mM EDTA. Antibody stocks were stored at -20°C in single use aliquots until use.

Once thawed, the samples were placed at 4°C for short-term storage. Quality control evaluation involved resolution via SDS/PAGE for reduced and non-reduced samples and flow cytometry for confirmation of binding affinity.

2.2.4 Fluorophore binding to glycoengineered antibody

DBCO-carboxyrhodamine was used to label the glycoengineered antibody. Fluorophore was incubated with the antibody at 37°C for 2hrs on a rotating platform (Barnstead International, Dubuque, IA). Unbound dye was removed by dye removal columns (Pierce, Rockford, IL). This process was carried out using both control and glycoengineered antibodies. Flow cytometry was used to confirm the binding of fluorophore to antibody. For flow cytometry, fluorophore conjugated, anti-perlecan antibodies were incubated with MDA-MB-231-LM2 cells and anti-CD133 antibodies were incubated with Caco2 cells at a concentration of 100 nM for 2 hours at 4°C on a rotating platform, followed by three washes using FACS Buffer. The cells were re-suspended in flow buffer and placed on ice until analysis by flow cytometry (BD LSRFortessa).

2.2.5 Biotin binding to glycoengineered antibody

DBCO-PEG4-biotin was incubated with the antibody at 37°C for 2hrs on a rotating platform. Unbound DBCO-PEG4-biotin was removed by AmiconÒ Ultra-4 Centrifugal filter units, 10KDa (Millipore Sigma, Burlington, MA). This process was carried out using both control and glycoengineered antibodies. Flow cytometry was used to confirm the binding of DBCOPEG4-biotin to the antibody. For flow cytometry, biotin conjugated, anti-perlecan antibodies were incubated with MDA-MB-231-LM2 cells and anti-CD133 antibodies were incubated with

Caco2 cells at a concentration of 100 nM for 1 hour at 4°C on a rotating platform, followed by three washes using FACS Buffer. Alexa Fluro 488 streptavidin (Life Technologies, Carlsbad, CA) was added to the cells and incubated at 4°C on a rotating platform, followed by three washes using FACS Buffer. The cells were re-suspended in flow buffer and placed on ice until analysis by flow cytometry. Biotin quantification kit (ThermoFisher Scientific) was used for quantification of number of biotin molecules conjugated per antibody.

2.2.6 Binding affinity of glycoengineered antibody

Flow cytometry was used to compare the binding affinity of glycoengineered antibody to that of control antibody. Anti-perlecan antibodies were incubated with MDA-MB-231-LM2 cells and anti-CD133 antibodies were incubated with Caco2 cells at a concentration of 100 nM for 1 hour at 4°C on a rotating platform, followed by three washes using FACS Buffer. Alexa Fluro 647 goat anti-human secondary antibody (Life

Technologies) was added and cells were incubated at 4°C on a rotating platform, followed by three washes using FACS Buffer. The cells were re-suspended in flow buffer and placed on ice until analysis by flow cytometry.

2.2.7 Tumor accumulation of glycoengineered antibody

This study was performed with anti-perlecan antibodies. Mice bearing MDA-MB-231-LM2 tumors (~300 mm^3) were injected with 100 μg of labeled isotype IgG control, anti-perlecan antibody (AM6 Ab) or glycoengineered anti-perlecan antibody (AM6-Az Ab) (n=3). Isotype IgG and AM6 Ab were labeled with Cy7 maleimide (Click Chemistry Tools) using immunothiolation to introduce reactive thiols onto the antibody. AM6-Az Ab was labelled with DNCO-Cy7 (Click Chemistry Tools, Arizona) using click chemistry. Mice were imaged using the IVIS Spectrum In Vivo Imaging System (University of Minnesota Imaging Centre) at various time intervals over 120 hours using excitation and emission filters of 750 nm and 775 nm, respectively. Data was acquired and analyzed using Living Image software. Data was tested for statistical significance using two way ANOVA, with multiple comparison *post-hoc* tests.

2.3 Results

2.3.1 Glycoengineered antibody shows presence of azide

To determine the presence of azide groups in glycoengineered antibodies, we incubated them with a fluorophore containing cyclooctyne group (DBCO-carboxyrhodamine). Binding of the dye conjugated antibodies to the target tumor cells was evaluated by flow cytometry. For anti-perlecan antibody, fluorescent signals were only observed in cells incubated with AM6-Az Ab. Cells incubated with AM6 Ab had signal similar to that of control cells (Figure 2.1 A). Similarly, for anti-CD133 antibody fluorescent signals were only observed in cells incubated with anti-CD133Az Ab and this signal was similar to the cells treated with commercial anti-CD133 Ab (Figure 2.1 B). Cells incubated with anti-CD133 Ab had signal similar to control cells (Figure 2.1 B).

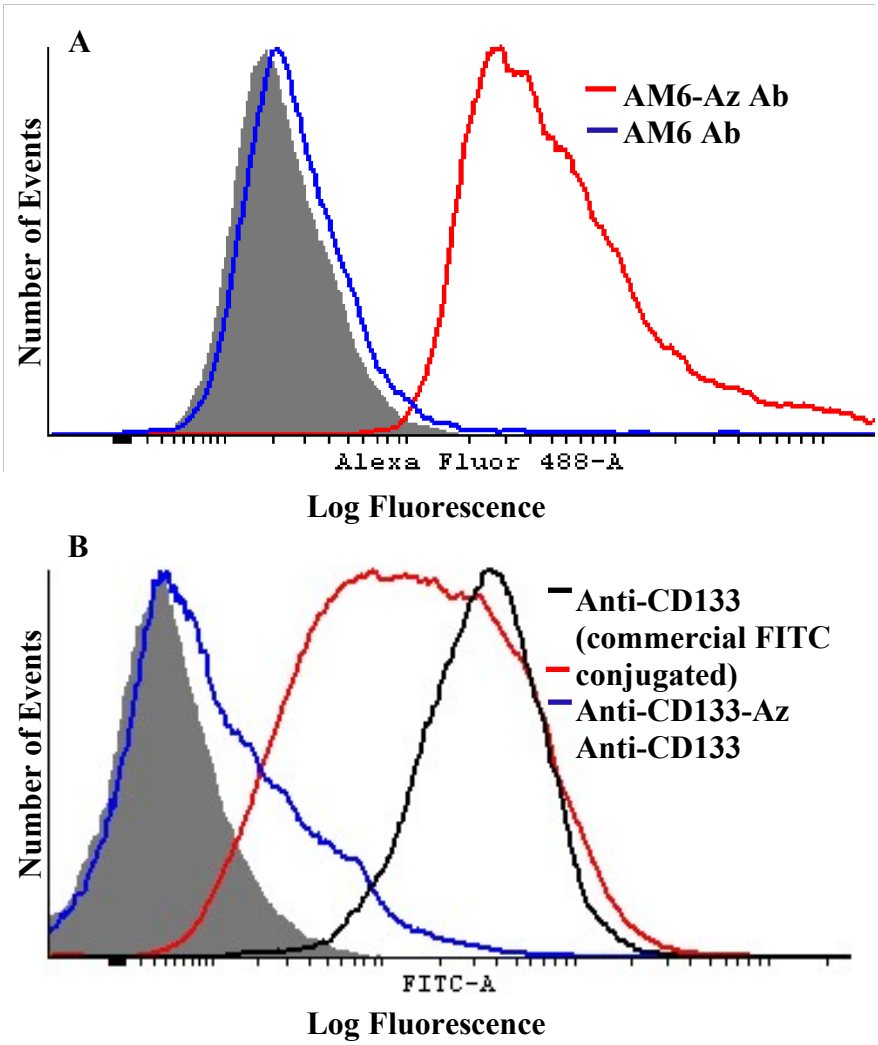

Figure 2.1: Dye labelled antibody binding to cells. **(A)** Histogram depicting flow cytometry data of anti-perlecan antibody in MDA-MB-231-LM2 cells. Glycoengineered anti-perlecan antibody showed fluorescent signals upon binding to cells. **(B)** Histogram depicting flow cytometry data of anti-CD133 antibody in Caco2 cells. Glycoengineered anti-CD133 antibody showed fluorescent signals upon binding to cells.

2.3.2 Quantification for number of azide groups

To quantify the number of azide groups per antibody, an indirect approach was used. We conjugated the glycoengineered antibody with DBCO-PEG4-biotin and then quantified the number of biotin molecules added to the antibody. After the conjugation of DBCO-PEG4-biotin to the antibodies, we first confirmed the presence of biotin by

flow cytometry using Alexa Fluro 488 streptavidin. For anti-perlecan antibody, fluorescent signal from streptavidin was only observed in cells incubated with AM6-Az Ab. Cells incubated with AM6 Ab had signal similar to control cells (Figure 2.2 A). Similarly, for anti-CD133 antibody, fluorescent signals were only observed in cells incubated with anti-CD133-Az Ab whereas cells incubated with anti-CD133 Ab had signal similar to control cells (Figure 2.2 B).

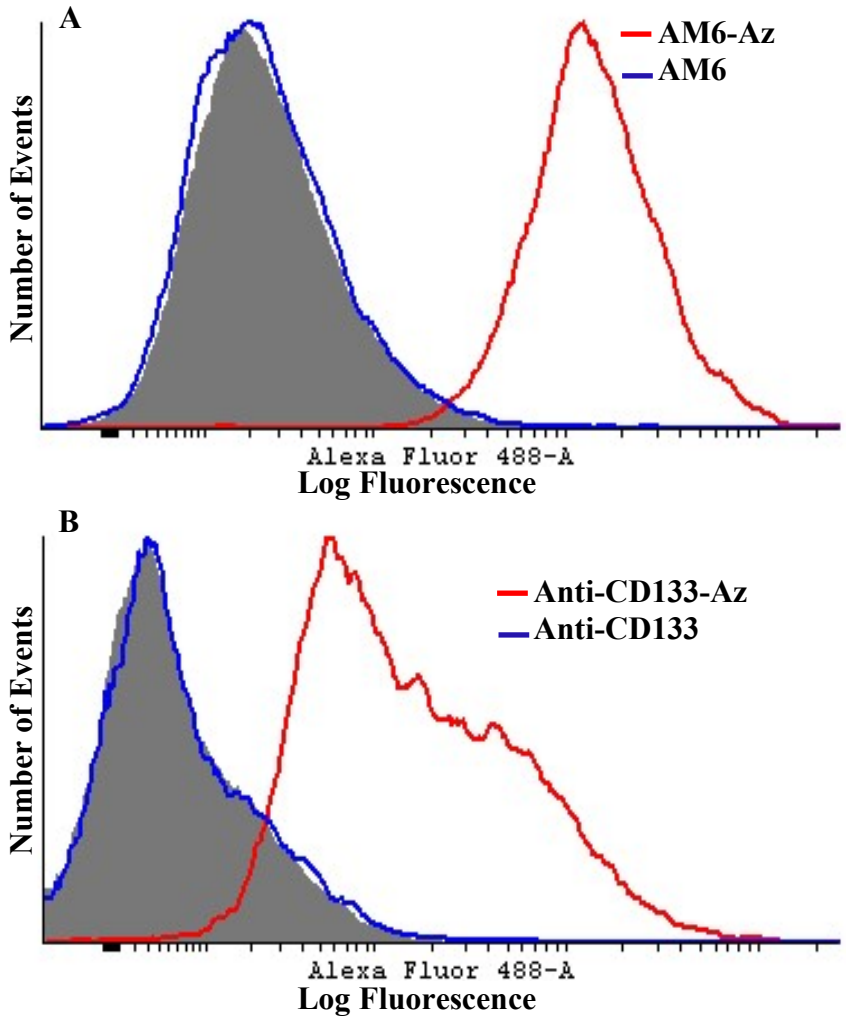

Figure 2.2: Biotinylated antibody binding to cells. **(A)** Histogram depicting flow cytometry data of anti-perlecan antibody in MDA-MB-231-LM2 cells. Glycoengineered anti-perlecan antibody showed presence of biotin. **(B)** Histogram depicting flow cytometry data of anti-CD133 antibody in Caco2 cells. Glycoengineered anti-CD133 antibody showed presence of biotin.

The biotinylated antibody was also used to quantify the number of biotin molecules per antibody by using biotin quantification kit. AM6-Az was found to contain 2.74 biotin molecules per antibody molecule while anti-CD133-Az antibody was labeled with 1.44 biotin molecules per antibody molecule. The number of biotin molecules present on each antibody molecule depends on the number of available azide groups, and so these parameters can be directly correlated. So, on an average, AM6-Az Ab had ~3 available azide groups per antibody and anti-CD133 Ab had ~2 available azide groups per antibody.

2.3.3 Glycoengineering does not affect binding affinity

To determine whether glycoengineering and conjugation to a payload affects the antigen binding affinity, we first stained the cells with glycoengineered biotinylated antibody or control unmodified antibody, followed by staining with a secondary antibody. For anti-perlecan antibody, fluorescent signals from the secondary antibody were similar for both biotinylated AM6-Az antibody or the unmodified AM6 Ab (Figure 2.3 A). Similarly, for anti-CD133 antibody, fluorescent signals from the secondary antibody were similar for biotinylated anti-CD133-Az, commercial anti-CD133 and anti-CD133 Ab (Figure 2.3 B). These results indicated that glycoengineering and conjugation of a payload does not affect the binding affinity of either of these antibodies for their respective target antigen.

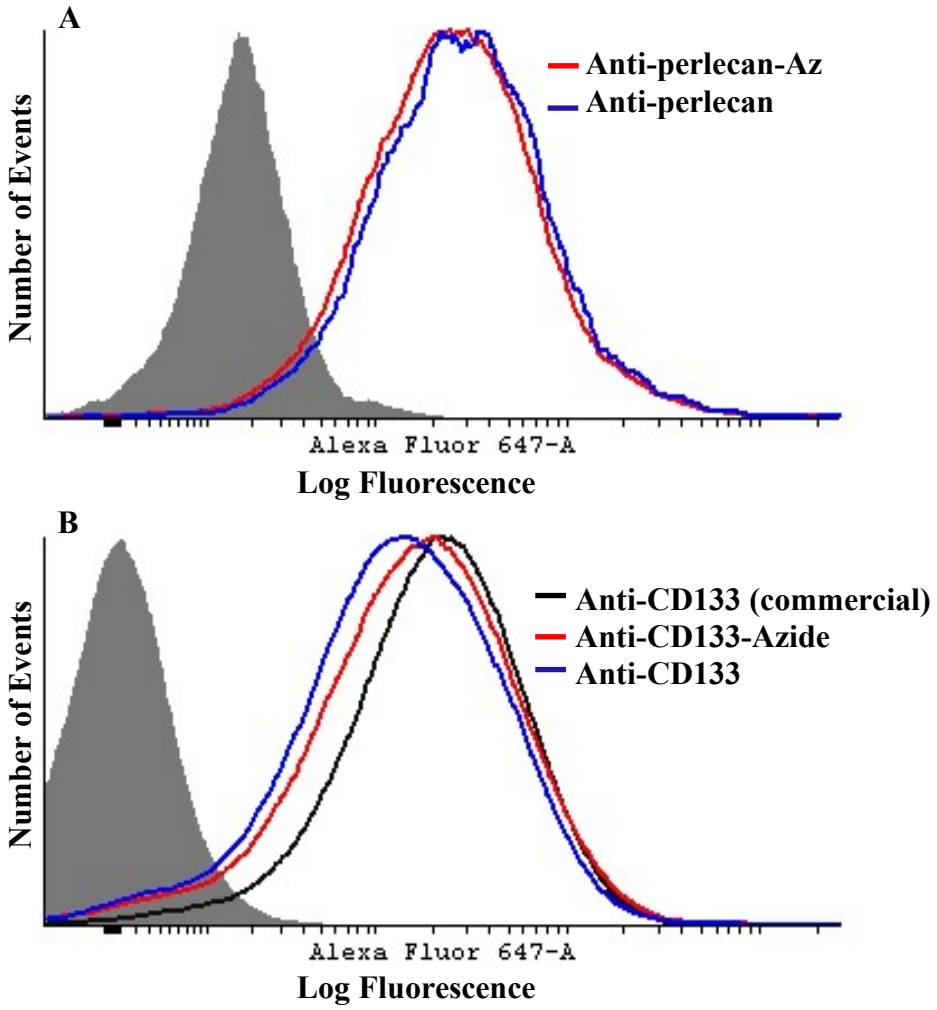

Figure 2.3: Binding affinity of antibody. **(A)** Histogram depicting flow cytometry data of antiperlecan antibody in MDA-MB-231-LM2 cells. Glycoengineered anti-perlecan and anti-perlecan antibody shows similar binding to cells. **(B)** Histogram depicting flow cytometry data of antiCD133 antibody in Caco2 cells. Glycoengineered anti-CD133, commercial anti-CD133 and antiCD133 antibody shows similar binding to cells.

2.3.4 Glycoengineered antibody accumulates in tumor

Previous studies in our lab have shown that anti-perlecan antibody specifically accumulates in xenografted MDA-MB-231 tumors. We determined whether glycoengineered anti-perlecan antibody demonstrated similarly enhanced tumor accumulation. An imaging study was carried out in tumor-bearing mice with fluorescently labeled glycoengineered and control AM6 antibodies. Following IV administration, significant accumulation of the fluorescent signal could be observed in the tumor starting at 24 hours. Quantitative analysis of fluorescence in the tumors revealed a 34 fold higher accumulation for both AM6-Az and AM6 Ab versus the isotype IgG control ($P<0.05$ at 3-24 hours, $p<0.001$ at 36-120 hour, two-way ANOVA with multiple comparisons) (Figure 2.4), This enhancement in tumor accumulation is similar to reports testing other tumor-targeting antibodies [95,96]. The Tmax in tumor for both AM6-Az and AM6 was 48 hours. This indicated that glycoengineered anti-perlecan antibody also accumulates in the tumor similar to unmodified antiperlecan antibody.

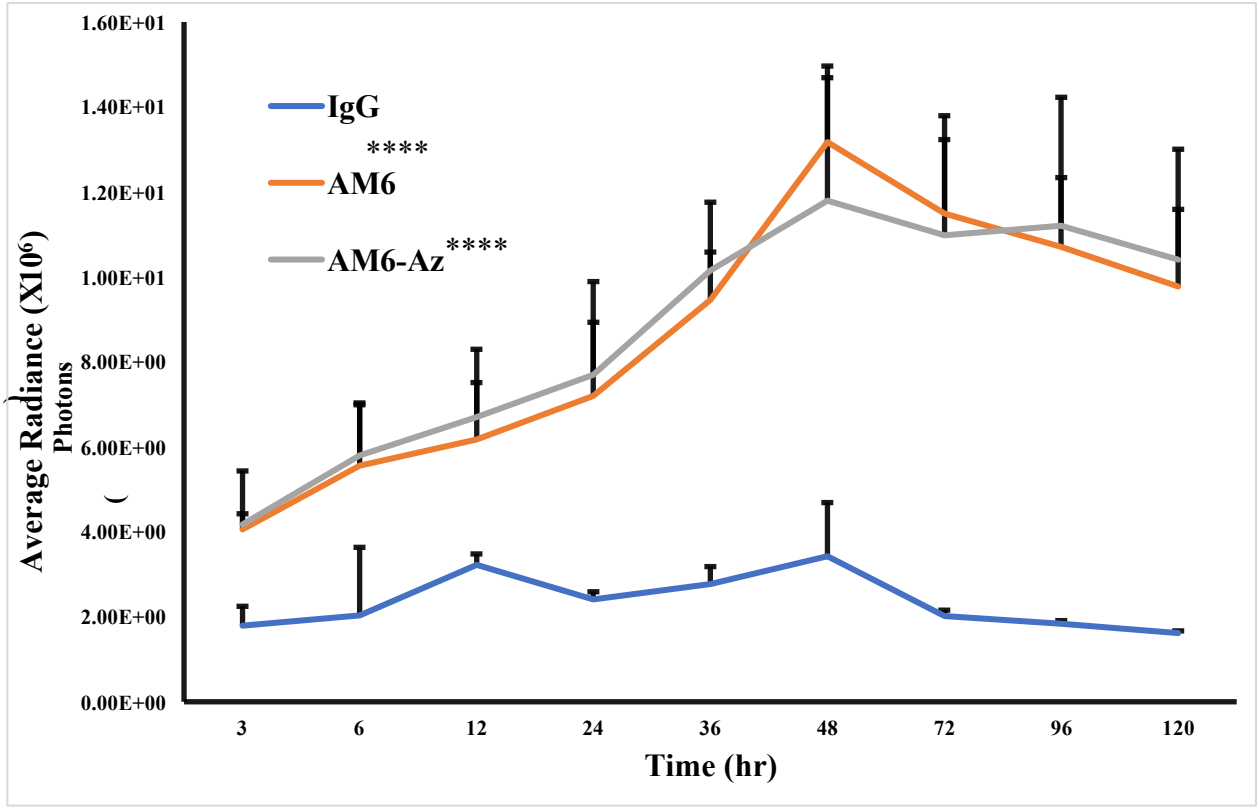

Figure 2.4: Antibody targeting *in vivo* by fluorescence-based imaging. Quantified fluorescence values in tumor post antibody administration. AM6-Az and AM6 Ab accumulated between 3-4-fold higher concentrations in the tumor (***P<0.001, two-way ANOVA with multiple comparisons, statistical significance is based on comparison between isotype IgG)

2.4 Discussion

The effector functions of monoclonal antibody are highly dependent on the structure of the Nlinked glycans in the Fc domain of the antibody and numerous investigations over past decades have evaluated methodologies to control the Fc glycan structures [7,94,97]. These include core fucosylation, terminal galactosylation and sialylation, as well as introducing high-mannose and bisecting glycans via multiple strategies [21]. There are a number of pros and cons for each of the many approaches [21].

These glycans have also been modified to introduce new functional groups including azides using chemo-enzymatic reactions on already expressed antibodies [92].

We hypothesized that substituting regular sugars in the cell culture medium with artificial sugars containing a reactive group is a simpler approach to change the glycoprofile of an antibody. After the production of glycoengineered antibodies, they were characterized for the presence of azide group by binding them to a fluorophore, DBCO-carboxyrhodamine. This fluorophore molecule consisted of a cyclooctyne group which will react with the azide molecule on the Nglycan of the glycoengineered antibody. The conjugation process was performed on control and glycoengineered antibody, but fluorescence signal was only seen from the cells treated with glycoengineered antibodies, indicating the presence of azide group.

To quantify the number of azide groups introduced in each antibody molecule using the glycoengineering strategu, we conjugated the glycoengineered antibodies with DBCO-PEG4biotin molecule and then quantified the number of biotin molecules conjugated to the antibody. The number of biotin molecules conjugated to the antibody correlates to the number of azide molecules available for conjugation. Using this correlation, we found that on an average, antiperlecan antibody had 2-3 molecules of available azide groups per antibody and anti-CD133 antibody had 1-2 azide groups per antibody. It has been reported that attaching a biomolecule can affect the antigen binding affinity of antibody [98]. So, we performed binding studies with the biotinylated antibodies and found no difference in binding affinity towards target antigen between control and glycoengineered antibodies. This indicates that glycoengineering and conjugation to a biomolecule does not affect the binding affinity towards target antigen.

It has been previously shown in our lab that anti-perlecan antibody accumulates in the tumor and in our studies, we found similar tumor accumulation of conventional and glycoengineered antibodies with Tmax of 48 hrs. Thus, the glycoengineering strategy can be used for incorporation of a reactive group on the antibody without affecting the tumor specificity of the antibody.

By using azido sugars, we were able to exploit the high reactivity of azide groups to any biomolecule containing a cyclooctyne group. We glycoengineered antibodies produced by two different production systems i.e., anti-perlecan antibody produced using Expi293F Expression System and anti-CD133 antibody produced by hybridoma cells. Thus, our studies show that glycoengineering strategy can be used for different production systems and for different antibodies. Additional optimization of this strategy may help in improving the number of available reactive groups per antibody.

2.5 Conclusion

A novel glycoengineering strategy was used to incorporate azide groups in the N-glycan region of two different antibodies without affecting the antigen binding or in vivo tumor accumulation of the antibody. Cyclooctyne containing payloads including fluorophores and PEG conjugates were successfully conjugated to glycoengineered antibodies. These results suggest that the glycoengineering strategy advanced here could be used to synthesize antibody conjugates for therapeutic and diagnostic applications.

Chapter 3: Use of glycoengineered antiperlecan antibody for synthesis of antibodydrug conjugates (ADC)

3.1 Introduction

The number of available carrier-based drug systems for the treatment of cancer and other diseases have seen an exponential growth in the past three decades. In addition, within the past 20 years, the use and approval of monoclonal antibodies (mAbs) has risen sharply, both in the clinic as well as in development. While early mAb therapies were plagued with toxicities due to immunogenicity, modern genetic engineering has led to human/humanized antibodies that are approved today [99]. Antibody–drug conjugates (ADCs) have emerged as the next generation anticancer therapeutic agents. ADCs harness the power of antibody specificity to target the delivery of highly potent drugs to the tumor site. Highly cytotoxic payloads are conjugated via linkers to tumor-targeting antibodies with an expectation of improved efficacy, safety, and, therefore, the therapeutic window of the cytotoxic payload.

Kadcyla and Adcetris are two FDA-approved ADCs that have shown remarkable clinical activities at well tolerated doses [100–102]. Kadcyla targets HER2-positive breast cancer with a maytansinoid DM1 conjugate [103], while Adcetris targets CD30-positive Hodgkin lymphoma with a monomethyl auristatin E (MMAE) conjugate [104]. A large number of other ADCs with various target antibodies, different linkers, and various payloads are now being tested in preclinical and clinical studies [105].

Currently used approaches to introduce therapeutic payloads rely primarily on conjugation to either side-chain amine or carboxylic acid groups or conjugation to thiols [92]. Because these reactions are not site-specific and not easily controlled, these chemistries can result in reduced affinity for the target antigen. Further, these

conjugation reactions lack selectivity and can result in heterogeneous mixtures of products that differ in the sites and stoichiometry of modification.

In this chapter, we present the results of our studies examining the use of glycoengineering strategy to synthesize ADCs

3.2 Methods

3.2.1 Materials

Cell culture supplies were obtained from Invitrogen (Waltham, MA) or Corning (Tewksbury, MA), unless otherwise specified. Fetal bovine serum (FBS) was purchased from Atlanta Biologicals (Flowery Branch, GA). N-azidoacetylgalactosamine-tetraacylated (Ac4GalNAz) sugar and DBCO-PEG12-MMAE was purchased from Click Chemistry Tools (Scottsdale, AZ).

Deionized (DI) water was available through university resources.

3.2.2 Cell Culture

MDA-MB-231-LM2 cells were from Joan Massague Laboraotry and have been previously described as being derived from lung metastasis arising from parental MDA-MB-231 tumors in mice. Cells between passages of 2 and 10 were used for all the studies. Cells were cultured in minimum essential medium (MEM) with 10% v/v fetal bovine serum (FBS) and 1% v/v penicillin/streptomycin in a humidified atmosphere with 5% CO_2.

3.2.3 Preparation and purification of glycoengineered anti-perlecan antibodies

Expi293F Expression System by Life Technologies (Carlsbad, CA) was used for the expression of anti-perlecan antibodies. During the process of production of antibody, 25 μM of Ac4GalNAz sugar was added to the cells with the enhancers a day

after transfection and also for subsequent three days. Control antibody was made without the addition of Ac4GalNAz sugar.

Seven days after transfection, affinity purification of antibodies was carried out using Protein A

Plus (Pierce, Rockford, IL) followed by buffer exchange into tris-buffered saline containing 5mM EDTA. Zeba^{TM} Spin Desalting Columns (87769, Pierce Biotechnology, Rockford, IL) were used for the buffer exchange step. Antibody stocks were stored at -20°C in single use aliquots until use. Once thawed, the samples were placed at 4°C for short-term storage. Quality control evaluation involved resolution via SDS/PAGE for reduced and non-reduced samples and flow cytometry for confirmation of binding affinity.

3.2.4 Preparation, purification and characterization of ADC

DBCO-PEG12-MMAE conjugated to glycoengineered anti-perlecan antibody by incubating the PEG-drug conjugate with the antibody at 4°C for 12 hrs on a rotating platform (Barnstead International, Dubuque, IA). Unbound Drug was removed by AmiconÒ Ultra-4 Centrifugal filter units, 10KDa (Millipore Sigma, Burlington, MA). ADC stocks were stored at -20°C in single use aliquots until use. Once thawed, the samples were placed at 4°C for short-term storage. Drug to antibody ratio (DAR) was determined by UV Vis spectroscopy using Nanodrop 2000c (ThermoFisher Scientific, Waltham, MA). This method was used as the UV/VIS spectra of the drug and of the antibody had different lmax values of 248 nm and 280 nm respectively [106]. Using the measured absorbances of the ADC and the extinction coefficients of the mAb at its lmax

of ~280 nm and the drug at its lmax of 248 nm, the individual concentrations of mAb and drug were determined by solving two simultaneous equations. From this, the molar ratio (moles of drug per mole of antibody) was calculated. The following are the equations used for calculation of DAR [107]:

$$A_{\#\$\%} = \in_{)}^{\#\$\%} C_{)}\, l + \in_{-.}^{\#\$\%} C_{-.} l$$

$$A_{\#/\$} = \in_{)}^{\#/\$} C_{)}\, l + \in_{-.}^{\#/\$} C_{-.} l$$

$$MR = \frac{\in_{-.}^{\#/\$} - R \in_{-.}^{\#\$\%}}{R \in_{)}^{\#\$\%} - \in_{)}^{\#/\$}}$$

where,

$\in^{\#\$\%}_{)}$, $\in^{\#/\$}_{)}$ = extinction coefficient of drug at 280 and 248nm

$\in^{\#\$\%}$, $\in^{\#/\$}$ = extinction coefficient of antibody at 280 and 248nm

$C_{-.}$ $_{-.}$ = = concentration of drug concentration of antibody

l = Detector path length

MR $= C_{)}/C_{-.}$ = Drug:Ab molar ratio

$R = A_{\#/\$}/A_{\#\$\%}$ = Absorbance ratio

3.2.4 Internalization of anti-perlecan antibody

Internalization and intracellular distribution of anti-perlecan antibody was determined by confocal laser scanning microscopy (Olympus FluoView FV1000 BX2 Upright Confocal,

Olmpus, Center Valley, PA). MDA-MB-231-LM2 cells (10000/chamber) were seeded into a

Lab-TekÒ Chamber SlideTM system (Sigma). The next day, the cells were

incubated with AM6-Az Ab (100 nM) labelled with DBCO-Cy 5.5 for 6 or 24 hours and then rinsed with PBS twice. Cells were counterstained with LysoTrackerÒ

Green (Thermo Scientific) and fixed with

3% paraformaldehyde (PFA), followed by staining with 4',6-diamidino-2-phenylindole (DAPI; Thermo Scientific). Confocal images were further analyzed by Olympus Fluoview viewer 2.0 software.

3.2.5 Cytotoxicity study with ADC

LM2 cells were seeded at 2500 cells per well in a 96-well plate and allowed to adhere overnight. Treatments (free MMAE, AM6 Ab or AM6-MMAE ADC) were added the next day at 125 nM equivalent MMAE concentration or 50 nM equivalent antibody concentration. The treatments were incubated for 6 hours, followed by removal of the treatments and addition of fresh media. Cell survival was analyzed at 48 hours using CellTiter 96 AQ_{ueous} One Solution Cell Proliferation Assay (Promega, Madison, WI).

3.2.6 Tumor growth inhibition study

MDA-MB-231-LM2 tumors were grafted in Balb/c homozygous nude mice (Jackson Labs). Once tumor volumes reached 100 mm^3, three doses of of the ADC at 3 mg/kg or 0.3 mg/kg were

administered through tail vein injection once every 96 hrs. Saline and equivalent dose of free drug and antibody (equivalent to 3mg/kg of ADC dose) were used as controls (n=7). Tumor volumes were measured every third day with digital Vernier calipers (Marathon Watch, Vaughn, Canada). Tumor volumes were calculated from the ellipsoid sphere equation $V = (L^2 * W)/2$, L being the longer measurement. Two way ANOVA, with multiple comparison post-tests, was used to determine the

statistical significance of the data.

3.3 Results

3.3.1 DAR of ADC

The glycoengineered anti-perlecan antibody AM6 was conjugated to a highly potent drug molecule, MMAE. Our previous studies demonstrated that glycoengineered AM6 has 2-3 azide groups per antibody (Section 2.3). The ADC constructed here with MMAE was found to have 2.56 MMAE molecules per molecule of antibody. Thus, this correlates well with the number of azide groups available for conjugation. For studies described below, the concentrations of ADC are reported based on the antibody concentration.

3.3.2 Anti-perlecan antibody shows slow internalization

As explained in Section 1.6.1, internalization of the ADC is a key determinant of efficacy while using non-cleavable linker technology for ADC. Insufficient internalization can prevent the cytotoxin from reaching the threshold concentration [108]. To confirm that the anti-perlecan antibody AM6 was indeed internalized by MDA-MB-231-LM2 cells after binding to the target surface antigen, we performed confocal microscopy studies. Cells were incubated with antibody for 6 hours and 24 hours, fixed and imaged after staining with DAPI (blue) and lysotracker (green) to visualize the nucleus and acidic endo/lysosomes, respectively. A majority of antibody was localized on the cell membrane after 6 hours. After 24 hours, a small fraction of the antibody was still localized on the cell membrane; however, a majority of the antibody was internalized. Antibody associated fluorescence was observed in the endo/lysosomes (shown by the presence of yellow fluorescence in the merged picture) and in the

nucleus (shown by the presence of pink fluorescence in the merged picture) (Figure 3.3). This data shows that anti-perlecan antibody is slowly internalized into cells.

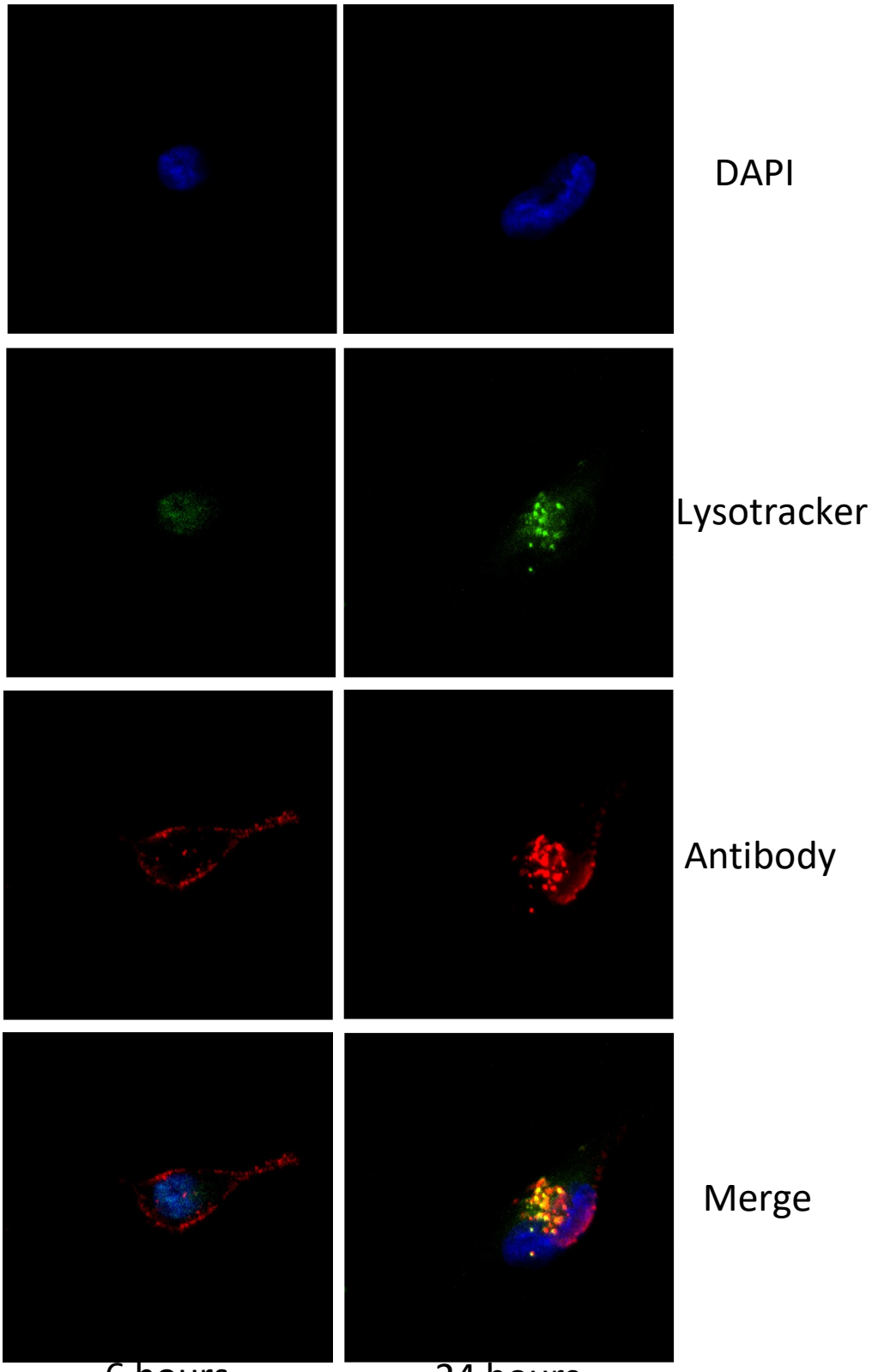
DAPI
Lysotracker
Antibody
Merge
6 hours
24 hours

Figure 3.1: Antibody internalization by confocal imaging. Blue: nucleus; Green: endo/lysosomes; red: anti-perlecan antibody. Scale bar, 5 um.

3.3.3 ADC kills cancer cells more effectively

In order to test the potency of the AM6-MMAE ADC, we first performed an *in vitro* cytotoxicity assay with MDA-MB-231-LM2 cells. At a concentration of 50 nM, treatment with ADC resulted in a significantly greater tumor cell kill as compared to that with an equivalent concentration of free MMAE (46% viability as opposed to 71% in case of MMAE, $P<0.05$, two way ANOVA with multiple comparison tests, Figure 3.1). We did not observe any cytotoxicity with just the AM6-Az antibody.

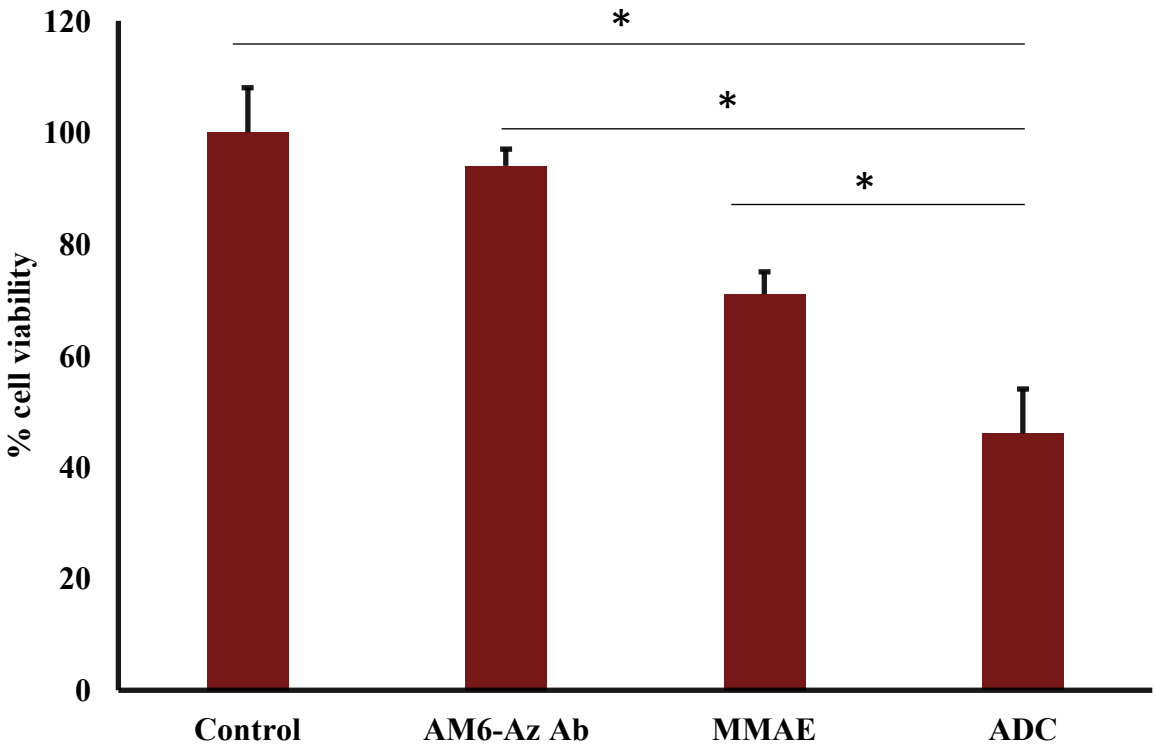

Figure 3.2: *In vitro* cytotoxicity study with MDA-MB-231-LM2 cells. ADC treated groups showed higher cytotoxicity (*$P<0.05$, two way ANOVA with multiple comparison tests, statistical significance is based off comparison between control cells, AM6-Az Ab and MMAE)

3.3.4 ADC is effective in inhibiting tumor growth in vivo

In order to determine the ability of ADCs to improve drug delivery *in vivo*, we tested the anticancer efficacy in the MDA-MB-231-LM2 orthotopic mouse tumor model (Figure 3.2). ADCs provide selective delivery of highly potent cytotoxic agent to cancer cells via specific binding of the antibody to cancer selective cell surface molecules [13]. Based on improved cytotoxicity of ADC relative to that of free drug, we tested two concentrations of ADC *in vivo*. We observed improved tumor growth inhibition with 3 mg/kg of ADC relative to equivalent dose of MMAE and AM6-Az Ab ($P<0.001$, two-way ANOVA with multiple comparisons, statistical significance is based on comparison between untreated, MMAE and AM6-Az Ab on the last day of the study). On the other hand, 0.3 mg/kg ADC also showed tumor inhibition relative to MMAE and AM6-Az Ab (dose was equivalent to 3mg/kg of ADC) ($P<0.05$, two-way ANOVA with multiple comparisons, statistical significance is based on comparison between untreated, MMAE and AM6-Az Ab on the last day of the study). On day 26, the untreated animals had an average tumor volume of ~1950 mm^3. Free MMAE and AM6-Az Ab showed around 18% tumor inhibition. On the other hand, 0.3 mg/kg ADC dose showed 26% tumor inhibition while 3 mg/kg ADC dose showed 55% tumor inhibition relative to that of untreated control at the end of the study.

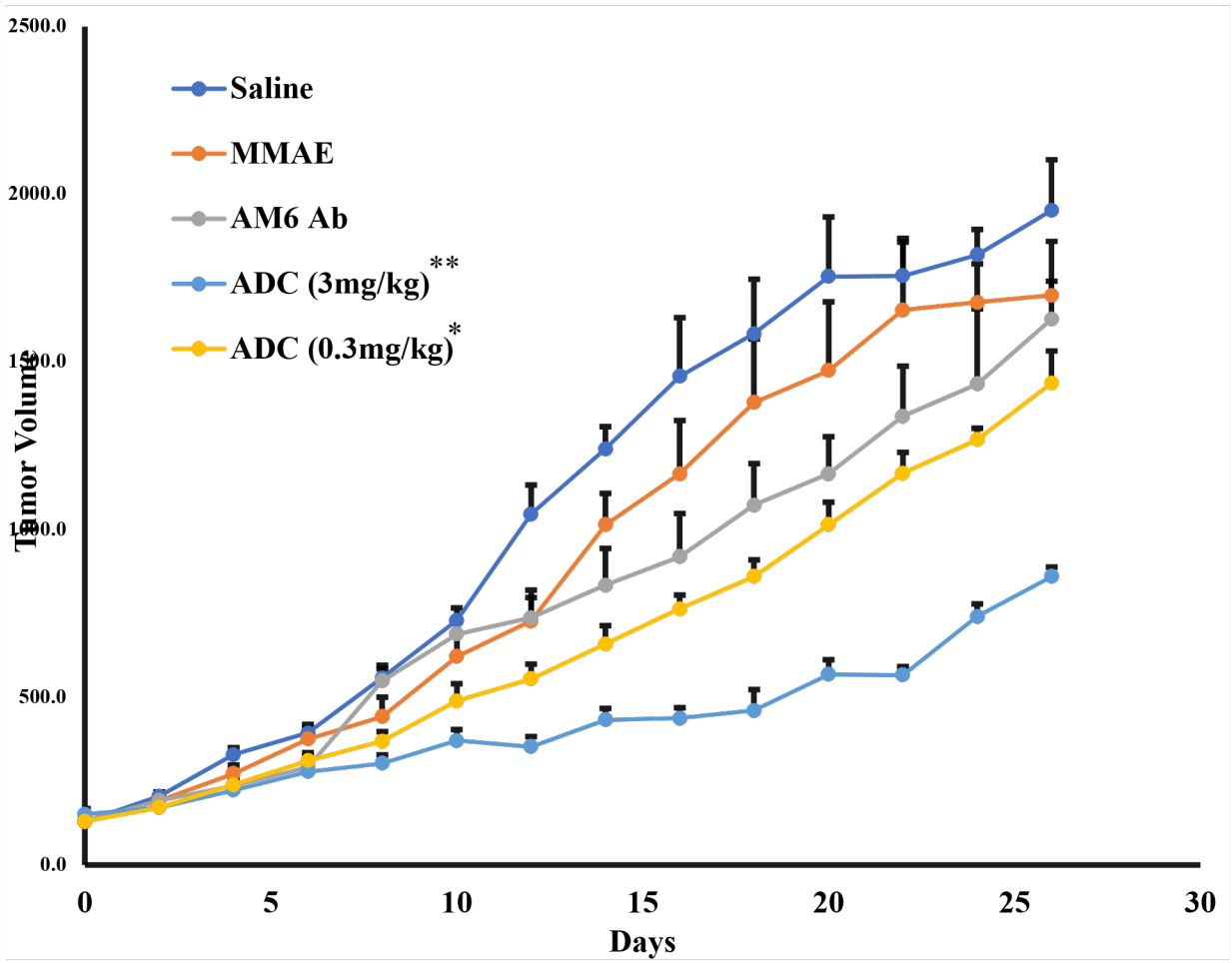

Figure 3.3: Efficacy study in Balb/c athymic nude mice. 3 mg/kg ADC showed significantly enhanced tumor inhibition over MMAE and AM6-Az Ab (**P<0.001, two-way ANOVA with multiple comparisons, statistical significance is based on comparison between untreated, MMAE and AM6-Az Ab on the last day of the study). 0.3 mg/kg ADC also showed significantly tumor inhibition over MMAE and AM6-Az Ab (*P<0.05, two-way ANOVA with multiple comparisons, statistical significance is based on comparison between untreated, MMAE and AM6-Az Ab on the last day of the study)

3.4 Discussion

Conjugation of drugs to antibodies has been performed through reactions with the activated carboxyl groups of N hydroxy succinimide (NHS) esters with lysine residues, or through the reactions of thiol-specific reagents, such as maleimide, with cysteines [109]. Lysine conjugation results in 0–8 drug molecules per antibody, and peptide mapping has determined that conjugation occurs on both the heavy and light chains at about 20 different lysine residues (~40 lysine residues are present per mAb). Therefore, more than one million different ADC species can be generated through this reaction [29]. For cysteine conjugation, the drug/antibody ratio (DAR) can range from 0 to 8; thus, generating more than 100 different ADC species [91]. However, several critical issues regarding the performance of ADCs prepared by the conventional methods are still being investigated. Several groups have reported that changing the number and position of the drug payload in the ADCs affects the pharmacokinetics, drug release rates, and biological activity [10,90].

Our strategy for site-specific antibody drug conjugation technology involves coupling the drug molecules to modified N297 glycans on the antibody. This approach is expected to generate sitespecific ADCs. Although the DAR achieved with this approach was 2-3, we expect that this can be further optimized to increase the available reactive groups present on the N297 glycan of the antibody. The AM6-MMAE ADC showed better antitumor efficacy compared to the controls in vitro as well as in vivo. As discussed in Section 1.6.1, linker technology is a critical parameter affecting the

efficacy of any ADC. In our studies, we used a non-cleavable PEG linker. So, the mechanism of action for this ADC likely involves binding to the cell surface antigen (perlecan) on the target cells, followed by slow internalization of the ADC into the endo-lysosomes. Lysosomal degradation of the antibody will allow for the release of the cytotoxic payload from ADC [108]. Because our internalization studies show that AM6 is slowly internalized, incorporation of a rapidly cleavable linker in the ADC could further improve its anticancer effectiveness.

3.5 Conclusion

Glycoengineered antibody was used to generate AM6-MMAE ADC with a DAR of 2-3 drug molecules per antibody. This ADC showed enhanced antitumor efficacy in vitro as well as in vivo. Cellular internalization studies suggest that incorporation of a cleavable linker in the ADC could further improve its anticancer effectiveness.

Chapter 4: Glycoengineered antibodies for surface functionalization of polymeric nanoparticles

4.1 Introduction

Nanoparticles (NPs) have been studied extensively as a drug delivery platform to overcome inherent limitations of conventional drugs including unfavorable pharmacokinetics, poor solubility and lack of target selectivity [110]. Numerous NP platforms including drug encapsulating polymeric NPs, self-assembling micellar NPs, and drug-polymer conjugates were developed to treat multiple diseases [111]. Application of NPs to treat cancer have so far shown promising preclinical activity but limited clinical success [22].

Discovery of the enhanced permeability and retention (EPR) effect [112], which explains enhanced accumulation of macromolecules via extravasation through leaky blood vessels in the tumor, led to an explosive increase in studies examining nanoparticles as a carrier for chemotherapy against solid tumors. Two notable examples of FDA approved nanomedicines are liposomal doxorubicin (Doxil) and albumin bound paclitaxel (Abraxane) [113,114]. To further improve NP accumulation and retention within tumors, a number of studies have focused on active targeting strategies that involve surface modification of the delivery system with a ligand capable of binding to components of a tumor. [3,115]. Currently used approaches to introduce targeting ligands on NPs rely primarily on conjugation via either side-chain amine or carboxylic acid groups or conjugation to thiols [92]. Because these reactions are not site-specific and not easily controlled, these chemistries can result in reduced affinity of the ligand for the target antigen.

In this chapter, we present the results of our studies examining the use of glycoengineering strategy to introduce tumor-targeting antibodies on the surface of polymeric nanoparticles. We utilized nanoparticles formulated from the biodegradable polymer, poly(D,L-lactide-co-glycolide) (PLGA), as they enable greater and sustained cellular delivery of encapsulated payload [116,117]. We formulated PLGA NPs that were surface functionalized with DBCO-terminated PEG chains and conjugated them to glycoengineered anti-perlecan antibody (AM6) using click chemistry. These perlecan targeted nanoparticles showed promising efficacy in *in vivo* models of triple negative breast cancer and non-muscle invasive bladder cancer.

4.2 Preparation and characterization of antibody conjugated nanoparticles

4.2.1 Method

4.2.1.1 Materials

PLGA (50:50, 0.55-0.75Dl/g) was purchased from LACTEL Absorbable Polymers (Birmingham, AL). The diblock copolymer polylactide-polyethylene glycol with terminal DBCO functionalization (PLA-PEG-DBCO) and rhodamine labeled PLGA (PLGA-
rhodamine) were purchased from PolySciTech (West Lafayette, IN). Polyvinyl alcohol (PVA, 30,000-70,000 MW), sucrose and ethylenediaminetetraacetic acid (EDTA) were purchased from Sigma (St. Louis, MO). Paclitaxel was purchased from Phytogen Life Science (B.C,
Canada). Control isotype IgG (Cat. No. 401114) was purchased from Calbiochem (Billerica, MA). The materials for SDS/PAGE were obtained from Bio-Rad (Hercules, CA). HPLC grade organic solvents were obtained from Fisher Scientific (Pittsburgh, PA). Cell culture media and buffers (including phosphate buffered saline, PBS) were purchased from Corning
(Tewksbury MA) or Life Technologies (Carlsbad, CA) unless otherwise specified. Deionized (DI) water was available through university resources.

4.2.1.2 Cell Culture

MDA-MB-231-LM2 cells were from Joan Massague Laboraotry and have been previously described as being derived from lung metastasis arising from parental MDA-MB231 tumors in mice. Cells between passages of 2 and 10 were used for all the studies. Cells were cultured in minimum essential medium (MEM) with 10% v/v fetal bovine serum (FBS) and 1% v/v penicillin/streptomycin in a humidified atmosphere with 5% CO_2.

4.2.1.3 Preparation of DBCO Functionalized PLGA Nanoparticles

PLGA nanoparticles surface functionalized with DBCO-terminated PEG and loaded with PTX were synthesized as described in an earlier publication [118], with minor modifications. PLGA (30 mg) and PTX (5mg) were dissolved in 1 ml of chloroform. An oil-in-water emulsion was formed by emulsifying the polymer-drug solution in 8 ml of 2.5% w/v aqueous PVA solution by probe sonication (18–24 W; Sonicator XL, Misonix, Melville, NY) for 5 minutes over an ice bath. PLA-PEG-DBCO (8 mg) was dissolved in chloroform (200 µl) and added dropwise to the above emulsion while the emulsion was stirred on a magnetic stirrer. The emulsion was stirred further for 16 -18 hours under ambient conditions followed by 1 hour under vacuum to remove the residual chloroform. Nanoparticles were washed twice by ultracentrifugation (35,000 rpm for 35 min at 4°C, Optima XPN-80, Beckman Palo Alta, CA) followed by reconstitution in DI water. The final nanoparticle dispersion was then stored at 4°C until it was used for conjugation reaction performed on the

same day. Rhodamine labeled nanoparticles were prepared similarly, except PLGA (25 mg) and PLGA-rhodamine (5 mg) were used instead of just PLGA.

4.2.1.4 Preparation and purification of glycoengineered anti-perlecan antibodies

Expi293F Expression System by Life Technologies (Carlsbad, CA) was used for the expression of anti-perlecan antibodies. During the process of production of antibody, 25 μM of Ac4GalNAz sugar was added to the cells with the enhancers a day after transfection and also for subsequent three days. Control antibody was made without the addition of Ac4GalNAz sugar. Seven days after transfection, affinity purification of antibodies was carried out using Protein A Plus (Pierce, Rockford, IL) followed by buffer exchange into trisbuffered saline containing 5mM EDTA. Zeba™ Spin Desalting Columns (87769, Pierce Biotechnology, Rockford, IL) were used for the buffer exchange step. Antibody stocks were stored at -20°C in single use aliquots until use. Once thawed, the samples were placed at 4°C for short-term storage. Quality control evaluation involved resolution via SDS/PAGE for reduced and non-reduced samples and flow cytometry for confirmation of binding affinity.

4.2.1.5 Conjugation of Antibody to Nanoparticles

AM6-Az Ab was buffer exchanged into PBS containing 5 mM EDTA (Zeba™ Spin Desalting Columns 87769). The desalted antibodies were immediately added to the nanoparticle dispersion and placed on a rotating platform at 4°C to allow the conjugation reaction to take place overnight. Next morning, nanoparticles were washed once by ultracentrifugation (35,000 rpm for 35 min at 4°C) and dispersed in 5

ml DI water containing 30 mg sucrose (lyoprotectant – reference Lin's paper). The final dispersion was probe sonicated (30 seconds, 6-9W) on an ice bath and centrifuged at 1000 RPM for 5 min to pellet any large aggregates. The supernatant was then lyophilized (Labconco, FreeZone 4.5, Kansas City, MO). The lyophilized product was stored in a desiccator at 4°C until further use.

4.2.1.6 Physiochemical Characterization of Nanoparticles

Hydrodynamic diameter and zeta potential of nanoparticles in DI water were determined using DelsaTM Nano C (Beckman Coulter Inc., Fullerton, CA, USA). To determine PTX loading, nanoparticles were dispersed in methanol (1 mg/ml) and incubated overnight at room temperature. The dispersion was then centrifuged at 13,000 RPM for 10 min and the supernatant was processed for HPLC analysis. Paclitaxel loading was determined using an HPLC method previously described [116]. HPLC was performed on a Beckman Coulter HPLC system equipped with a System Gold 508 autosampler was used. A Beckman Coulter C18 column (4.6 mm x 150 mm, 5 μm) was used as the stationary phase. The mobile phase consisted of a mixture of ammonium acetate (10 mM, pH 4.0) and acetonitrile in 45:55 ratio, and was delivered at a flow rate of 1 ml/min. A 50 μl volume of the methanol extract was injected using an autoinjector (Model 508, Beckmann Instruments). Paclitaxel was quantified by UV detection at 228 nm (System Gold 168 detector).

4.2.1.7 Confirmation of Antibody Conjugation and Loading

One milligram of nanoparticles was dispersed in 40 µl DI water and analyzed for protein concentration using bicinchoninic acid assay (Pierce BCA Protein Assay, Rockford, IL). In order to confirm chemical conjugation of the antibody to nanoparticles we used a gel electrophoresis technique (Swaminathan et al. 2013). One milligram of nanoparticles was suspended in 25 µl DI water. To each tube, 25 µl of 95:5 2X Gel Loading Buffer:2Mercaptoethanol (reduced samples) or 25µl of 2X Gel Loading Buffer (non-reduced samples) was added. The samples were placed in a water bath at 90°C for 10 min, centrifuged at 13,000 RPM for 10 min and the supernatants were resolved on a 4-10% SDS/PAGE Criterion Precast Gel (Bio-Rad, Hercules, CA), along with the respective antibody controls.

4.2.2 Results

4.2.2.1 Physiochemical characterization of antibody conjugated nanoparticles

Average hydrodynamic size of nanoparticles was ~350 nm as measured using DLS. Zeta potential was in the range of -12 mV. Presence of antibody did not influence the particle size or zeta potential to a significant extent. Paclitaxel encapsulation efficiency was greater than 90% and loading was 150 μg/mg of nanoparticles. Antibody concentration was between 5-10 μg/mg of nanoparticles, which translates into approximately 15-20 antibody molecules/nanoparticle (Table 1).

Table 1: Physicochemical characterization of nanoparticles

Characteristics	Anti-perlecan-Az NP	Blank NP
Nanoparticle Size	364.2 ± 24.8 nm	337 ± 38.3 nm
Zeta Potential	-12.7 ± 2.7mV	-11.9 ± 3.6mV
Protein Loading	7 ± 3 μg protein/mg NPs	-
Protein Encapsulation Efficiency	75 ± 25 %	-
Paclitaxel Loading	15.5% ± 1.7	15.1% ± 2.5

Antibody conjugation to nanoparticles was determined to be between 7 ± 3 μg protein/mg nanoparticles. BCA is able to provide information only about the presence

or absence of protein. In order to confirm covalent conjugation of the antibody to nanoparticles, we analyzed the nanoparticles using SDS/PAGE. 2-mercaptoethanol was used to reduce the thiol bonds between the heavy and light chains of the antibody. Nanoparticles were incubated under reducing conditions and the reduced samples were analyzed using SDS/PAGE. The azide alkyne bond is resistant to reduction by 2-mercaptoethanol. Thus, when antibody conjugated nanoparticles are subjected to a reduction step, only half the antibody molecule is expected to be released from the surface of nanoparticles (either the light chain or the heavy chain, depending on which is attached to the particle surface). If no reduction step is present, the antibody should not be released at all. We were able to confirm this with anti-perlecan-Az antibody conjugated nanoparticles (Figure 4.1). Lane 3 represents antibody-conjugated nanoparticles that were reduced, and thus we see bands at 25 kDa corresponding to the antibody light chains. Lane 4 represents non-reduced antibody-conjugated nanoparticles – no bands were observed in this case.

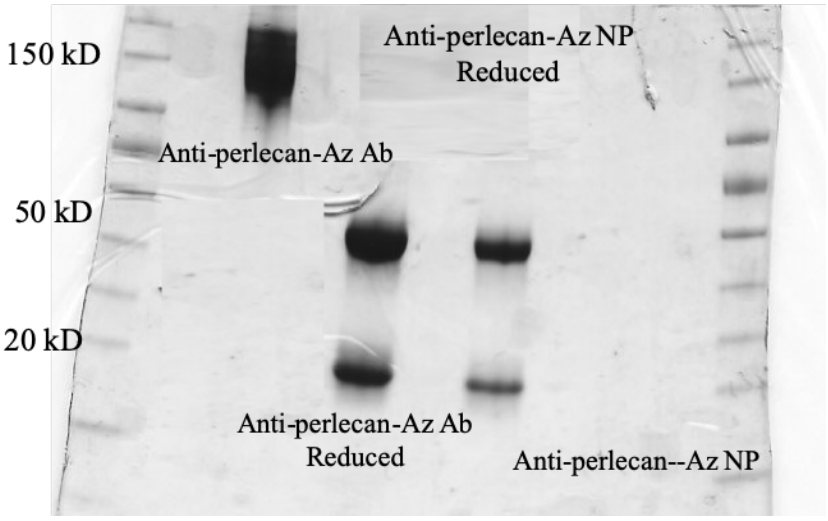

Figure 4.1: SDS/PAGE image showing the presence of antibody in anti-perlecan-Az NP

4.3 Perlecan-targeted nanoparticles for improved efficacy against triple negative breast cancer

4.3.1 Method

4.3.1.1 Materials

The materials for SDS/PAGE were obtained from Bio-Rad (Hercules, CA). HPLC grade organic solvents were obtained from Fisher Scientific (Pittsburgh, PA). All cell culture media and buffers (including phosphate buffered saline or PBS) were purchased from Corning (Tewksbury MA) or Life Technologies (Carlsbad, CA) unless otherwise specified. Deionized (DI) water was available through university resources.

4.3.1.2 Cell culture

MDA-MB-231-LM2 cells were from Joan Massague laboraotry and have been previously described as being derived from lung metastasis arising from parental MDA-MB231 tumors in mice. Cells between passages of 2 and 10 were used for all the studies. Cells were cultured in minimum essential medium (MEM) with 10% v/v fetal bovine serum (FBS) and 1% v/v penicillin/streptomycin in a humidified atmosphere with 5% CO_2.

4.3.1.3 Cell uptake of antibody conjugated nanoparticles

PTX loaded nanoparticles were used for this study. MDA-MB-231-LM2 cells were seeded at 50,000 cells per well in a 24-well plate and allowed to adhere overnight.

Cells were washed once with PBS and fresh media was added. The cells were incubated at 4°C for 2 hours with

PTX loaded nanoparticles at a final concentration of 100 μg/ml to allow binding to the target (n=4). At the end of 2 hours, the media was replaced with fresh media and the cells were placed at 37°C to allow internalization. The cells were lysed at 60 minutes post addition of treatments using 100 μL RIPA buffer. Part of the cell lysate (30 μL) was used to determine protein concentration by BCA assay and the rest was processed for HPLC analysis. PTX was extracted into 0.5 mL methanol overnight. The samples were centrifuged at 13,000 RPM for 10 min and the supernatant was analyzed for PTX concentrations using HPLC [116].

4.3.1.4 Cytotoxicity study

MDA-MB-231-LM2 cells were seeded at 2500 cells per well in a 96-well plate and allowed to adhere overnight. Treatments (free paclitaxel or paclitaxel loaded nanoparticles) were added the next day at concentrations equivalent to 50 nM paclitaxel. The treatments were incubated for 6 hours, followed by removal of the treatments and addition of fresh media. Cell survival was analyzed at 72 hours using CellTiter 96 AQueous One Solution Cell Proliferation Assay (Promega, Madison, WI).

4.3.1.5 Tumor growth inhibition study

MDA-MB-231-LM2 tumors were grafted in Balb/c homozygous nude mice (Jackson Labs). Once tumor volumes reached 100 mm^3, three doses of treatments equivalent to 40 mg/kg of PTX were administered through tail vein injection once

every 96 hrs. Free drug, nanoparticles without the targeting ligand (PEG NP) and saline were used as controls (n=7). Tumor volumes were measured every third day with digital Vernier calipers (Marathon Watch, Vaughn, Canada). Tumor volumes were calculated from the ellipsoid sphere equation $V = (L^2 * W)/2$, L being the longer measurement. Two-way ANOVA, with multiple comparison post-hoc tests, was used to determine the statistical significance of the data.

4.3.2 Results

4.3.2.1 Cell Uptake of Antibody Conjugated Nanoparticles

Uptake of antibody-conjugated nanoparticles was studied in MDA-MB-231-LM2 cells, which have been previously established in our laboratory as a perlecan positive cell line [120]. Presence of the antibody improved internalization of nanoparticles into cells as observed by cell uptake data (Figure 4.2). We saw a 2- and 3.5-fold improvement in uptake of targeted NP compared to control isotype IgG-conjugated NP ($P<0.05$) and control PEG NP ($P<0.05$),

respectively.

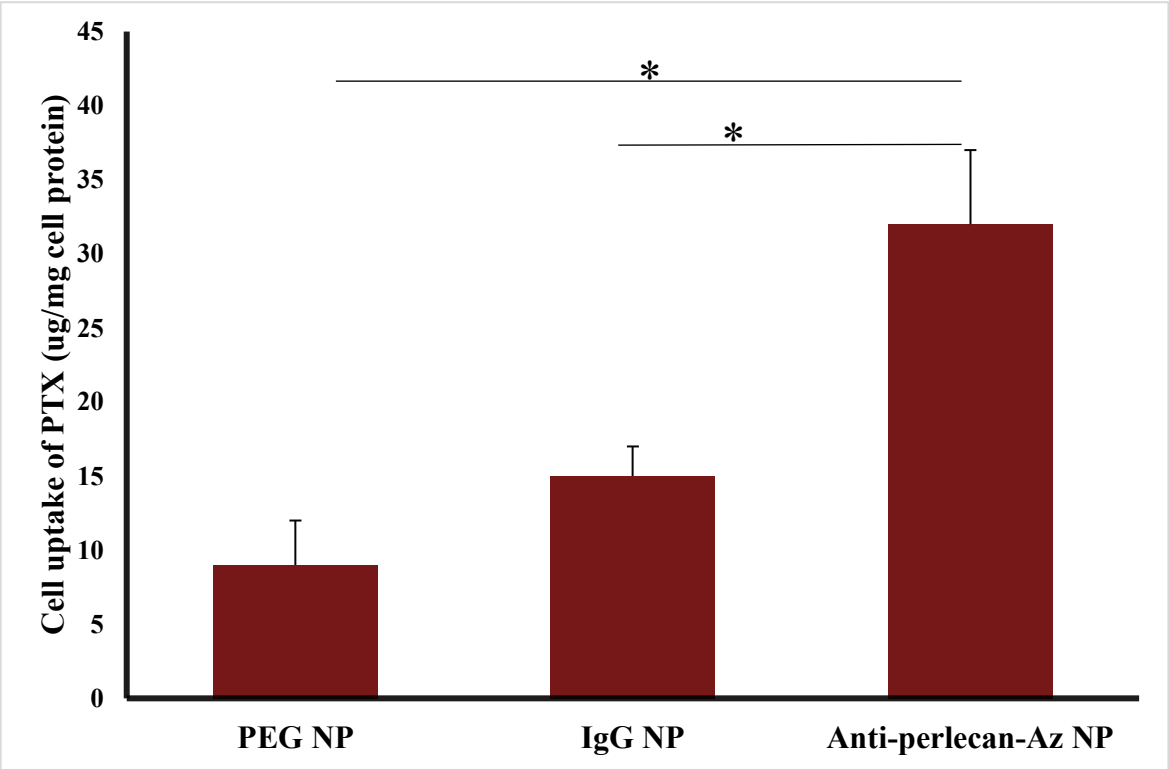

Figure 4.2: NP *In vitro* NP uptake with MDA-MB-231-LM2 cells. Cells incubated with antiperlecan-Az NP showed higher uptake (*P<0.05, two way ANOVA with multiple comparison tests, statistical significance is based off comparison between PEG NP and IgG NP)

4.3.2.2 In vitro cytotoxicity with antibody conjugated nanoparticles

In order to test the potency of targeted nanoparticles, we performed an *in vitro* cytotoxicity assay with MDA-MB-231-LM2 cells. Treatment with targeted nanoparticles resulted in a significantly greater tumor cell kill as compared to the equivalent concentration of non-targeted PEG NP and free drug (38% viability as opposed to 64% and 53% for PEG NP and PTX,

respectively) (P<0.05, Figure 4.3).

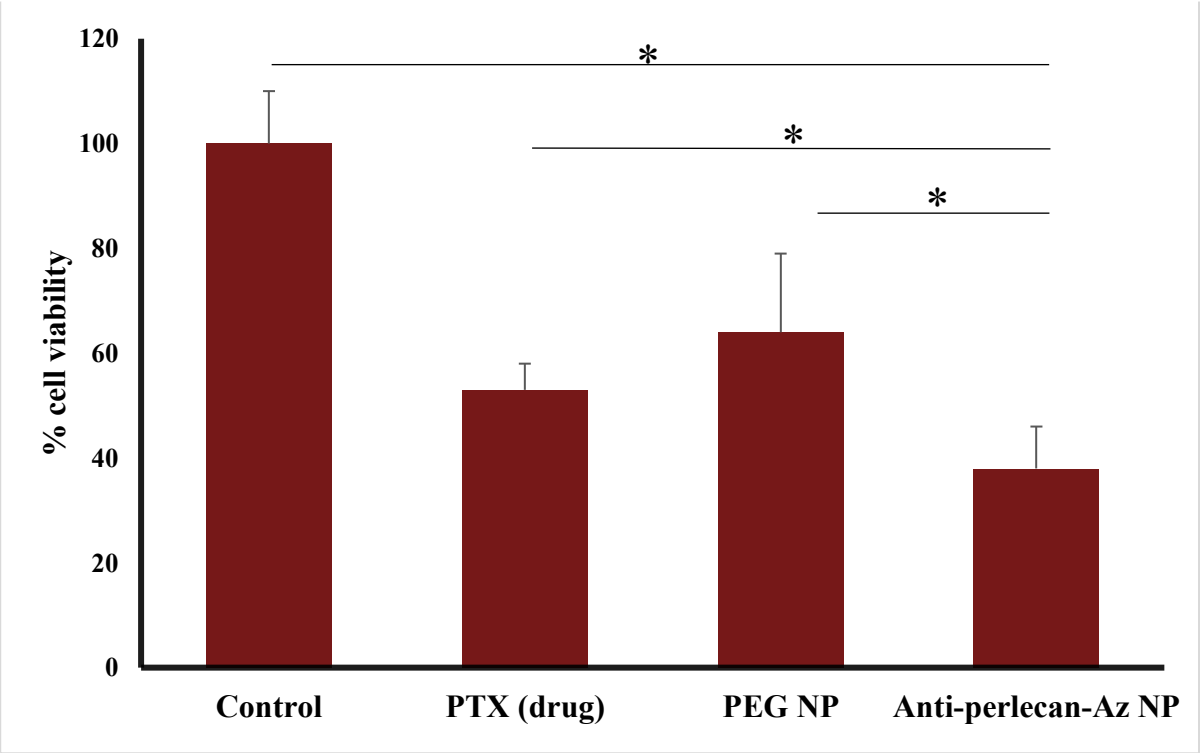

Figure 4.3: : *In vitro* cytotoxicity study with MDA-MB-231-LM2 cells. Anti-perlecan-Az NP treated groups showed higher cytotoxicity (*P<0.05, two way ANOVA with multiple comparison tests, statistical significance is based off comparison between control cells, PTX and PEG NP)

4.3.2.3 Antibody conjugated nanoparticles result in improved efficacy

In order to determine the ability of antibody conjugated nanoparticles to improve tumortargeted drug delivery *in vivo*, we tested the efficacy of targeted nanoparticles in the MDA-MB231-LM2 orthotopic mouse tumor model (Figure 4.4). Nanoparticles are known to have improved accumulation in the tumor due to the enhanced permeability and retention (EPR) effect [121]. Because of their ability to bind with and get internalized into tumor cells, targeted nanoparticles have greater retention in tumors in addition to the EPR effect [79,80]. We observed improved tumor growth inhibition with perlecan-targeted

nanoparticles relative to that with free drug and nontargeted PEG NP ($P<0.001$, statistical significance based on comparison between untreated, free drug and PEG NP on the last day of the study). On day 28, the saline, PTX and PEG NP treated animals reached an average tumor volume of ~1950 mm^3. Only targeted nanoparticles demonstrated tumor inhibition at the end of the study.

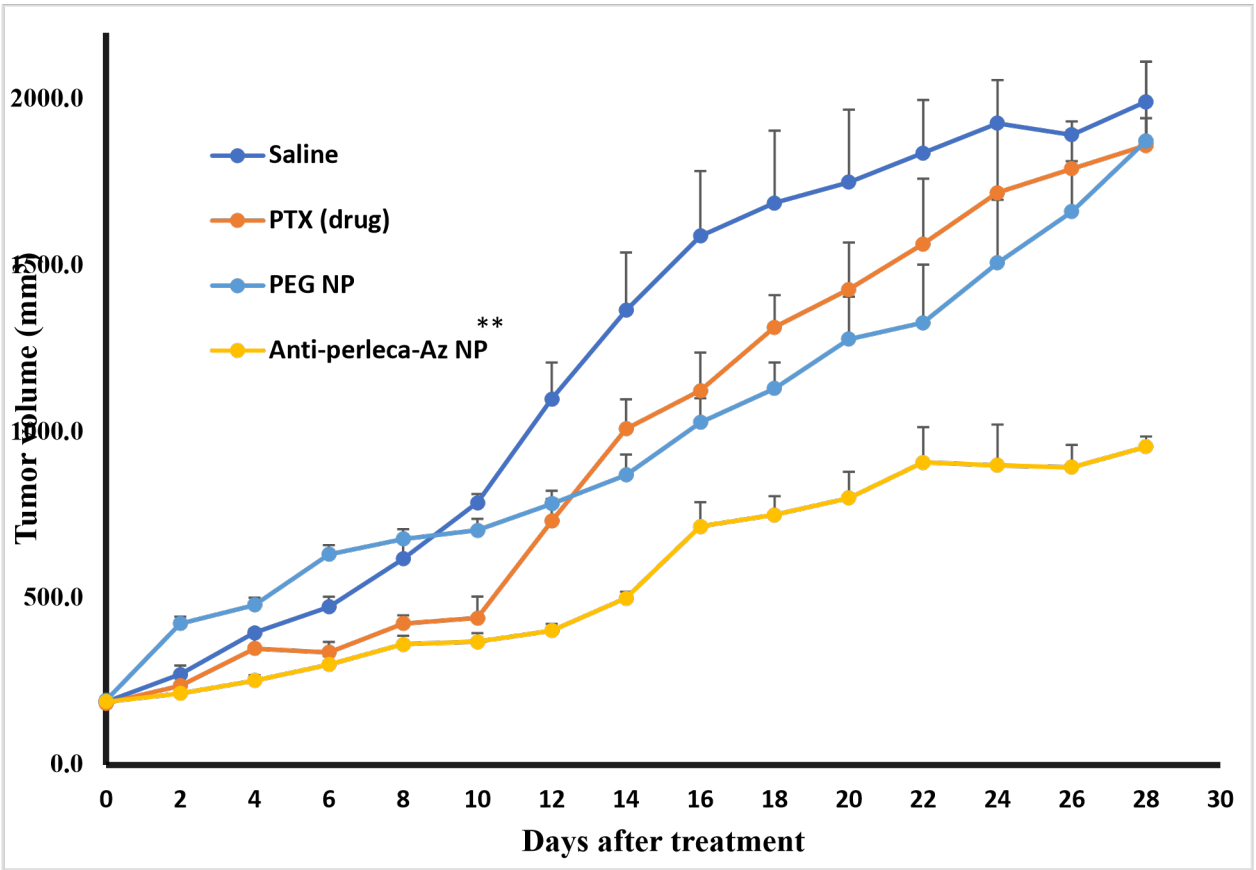

Figure 4.4: Efficacy study in Balb/c athymic nude mice. 40 mg/kg anti-perlecan-Az NP showed significantly enhanced tumor inhibition over PTX and PEG NP (**P<0.001, two-way ANOVA with multiple comparisons, statistical significance is based on comparison between untreated, MMAE and AM6-Az Ab on the last day of the study).

4.4 Perlecan-targeted nanoparticles for improved efficacy against bladder cancer

4.4.1 Method

4.4.1.1 Materials

HPLC grade organic solvents were obtained from Fisher Scientific (Pittsburgh, PA). Cell culture media and buffers (including phosphate buffered saline, PBS) were purchased from

Corning (Tewksbury MA) or Life Technologies (Carlsbad, CA) unless otherwise specified.

Deionized (DI) water was available through university resources.

4.4.1.2 Cell Culture

MB49 and MB49-luc (murine bladder cancer) cells were a gift from Thomas Griffith at the

University of Minnesota. Cells were cultured in RPMI 1640 with 10% v/v fetal bovine serum (FBS) and 1% v/v penicillin/streptomycin in a humidified atmosphere with 5% CO_2. Human bladder cancer cell lines, RT4 and T24, were also a gift from Thomas Griffith at the University of Minnesota. These cells were cultured in RPMI 1640 with 10% v/v fetal bovine serum (FBS) and 1% v/v penicillin/streptomycin in a humidified atmosphere with 5% CO_2.

4.4.1.3 Binding of glycoengineered anti-perlecan antibodies to bladder cancer cell lines

Flow cytometry was carried out to confirm that anti-perlecan antibody AM6 binds to bladder cancer cells. The antibodies were incubated with MB49, RT4 or T24 cells at a concentration of 100 nM for 1 hour at 4°C on a rotating platform (Barnstead International, Dubuque, IA). The cells were then washed three times using FACS Buffer (PBS containing 0.5% BSA, 2mM EDTA and 0.05% sodium azide). Alexa 647 goat anti-human secondary antibody (Life Technologies, Carlsbad, CA) was added and the cells were incubated at 4°C for one 1 hour on a rotating platform. Finally, the cells were washed three times, re-suspended in FACS buffer and placed on ice until analysis by flow cytometry (BD LSRFortessa).

4.4.1.4 Cell Uptake of Antibody Conjugated Nanoparticles analyzed by flow cytometry

Rhodamine labeled nanoparticles were used for this study. MB49 cells suspended in FACS buffer (200,000 cells in 150 µL) were incubated with 50 µg of nanoparticles (what is the volume?) on a rotating platform at 37°C for 1 hour (n=2). At the end of one hour, the cells were washed twice using FACS Buffer, fixed using 4% v/v formaldehyde in FACS Buffer, washed once followed by analysis using flow cytometry. Flow cytometry analysis was carried out using BD LSRFortessa H0081. Mean fluorescence intensity (MFI) from flow cytometry analysis was normalized to rhodamine loading in nanoparticles by using fluorescence of the nanoparticle

suspensions measured using the IVIS Spectrum in vivo Imaging System (Caliper Lifesciences, Hopkinton, MA).

4.4.1.5 Cytotoxicity Study

MB49 cells were seeded at 2500 cells per well in a 96-well plate and allowed to adhere overnight. Treatments (free paclitaxel or paclitaxel loaded nanoparticles) were added the next day at concentrations equivalent to 50 nM paclitaxel. The treatments were incubated for 6 hours, followed by removal of the treatments and addition of fresh media. Cell survival was analyzed at 72 hours using CellTiter 96 AQueous One Solution Cell Proliferation Assay (Promega, Madison, WI).

4.4.1.6 Development of orthotopic non-muscle invasive bladder cancer model

Female C57BL/6 mice (Charles River Laboratories, Wilmington, MA, USA), 5 weeks old, were used for developing orthotopic non-muscle invasive bladder cancer model. Urethral catheterization in mice under isoflurane was performed using a sterile 24 G pediatric venous catheter. Following urethral catheterization bladder walls were coated with poly-l-lysine (0.05 mL of 0.1 mg/mL) for 5 mins. Bladder was then washed with PBS followed by instillation of 0.5×10^6 cells MB49-luc cells (0.05 mL) through the urethral catheter for 55 min. Tumors were visualized by bioluminescence imaging using the IVIS Spectrum In Vivo Imaging System (University of Minnesota Imaging Centre).

4.4.1.7 Tumor growth inhibition study

MB49-luc non-muscle invasive bladder tumors were grafted in C57/bl6 mice (Charles River Labs). Once tumor volumes reached bioluminescence of 10^4 photons/sec, three doses of 40 mg/kg of PTX were administered through either tail vein injection (IV) or directly into the bladder via urethral catheter (IT) once every 96 hrs. Isotype IgG-conjugated non-targeted NP and saline were used as controls (n=6). Tumor volumes were monitored by bioluminescence imaging using the IVIS Spectrum In Vivo Imaging System (University of Minnesota Imaging Centre). Two-way ANOVA, with multiple comparison *post-hoc* tests, was used to determine the statistical significance of the data.

4.4.1.8 Immunohistochemistry (IHC)

At the end of the tumor growth study, mice were sacrificed. Bladders were excised and formalin fixed for 24 hours. The tissues were then transferred to 70% ethanol until processed.

The samples were submitted to the University of Minnesota Comparative Pathology Shared Resource for IHC processing. The sections were stained for Caspase 3 and Ki67. The IHC slides were submitted to the University of Minnesota Imaging Centre for slide scanning. Three snippets of approximately 1700 μm x 800 μm size were selected at random in the slide field, at 10X magnification and quantified for positive staining using the software ImageJ (NIH).

4.4.1.9 Accumulation of PTX in bladder

Orthotopic non-muscle invasive bladder cancer was established in C57/bl6 mice as described previously. One week following cell injection, animals were randomly assigned to various treatment groups. Targeted and non-targeted nanoparticles formulations (40 mg/kg of PTX) were administered either via the tail vein (IV) or directly into the bladder via urethral catheter (IT). Cohorts of mice were sacrificed at 0.5 h, 1 h, 2 h, 6 h or 24 h after treatment administration. Bladder, liver, kidney and spleen were collected and weighed. The organs were homogenized with PBS containing 5% BSA and lyophilized. Paclitaxel was extracted from the lyophilized organs using methyl tert-butyl ether. The ether was separated from the tissue homogenate by centrifugation and evaporated to dryness under nitrogen. The dried samples were reconstituted in methanol, centrifuged (14000 RPM, 15 min), and transferred to HPLC vials. Paclitaxel concentration was analyzed using LC-MS/MS as described before [86].

LC-MS/MS was performed on an Aquity UPLC (Waters) coupled with Micromass Quattro Ultima LC/MS/MS (Waters) was used. A Zorbax Eclipse XDB-C18 (50 x 4.6 x 1.8 mm) was used as the stationary phase. The mobile phase consisted of a mixture of water and methanol in 25:75 ratio with 0.1% formic acid (v/v), and was delivered at a flow rate of 0.4 ml/min. A 5 µl volume of the methanol extract was injected and autosampler temperature was maintained at 10°C. Mass spectrometric detection of PTX and IS (Docetaxel) was carried out in positive ion mode using a triple-quadrupole mass spectrometer (Waters), equipped with an electrospray ionization interface operating at a capillary voltage of 3 kV and cone voltage of 50 V. The collision energy

was set at 33 V for PTX and 30 V for IS. Detection of the ions was performed in multiple-reaction monitoring mode, monitoring the transition ion pair m/z 876.22/ 307.91 for PTX and m/z 830.16/548.97 for the IS. The dwell time per transition was 0.4 sec for both PTX and IS. Data acquisition and peak integration were achieved by MassLynx software, version 4.1.

4.4.2 Results

4.4.2.1 Anti-perlecan antibody binds to bladder cancer cell lines

It has been previously established in our lab that bladder cancer has high perlecan expression [120]. We carried out a flow cytometry experiment to determine the expression of perlecan in various bladder cancer cell lines. We found that anti-perlecan-Az antibody binds to human bladder cancer cell lines RT4 and T24 (Figure 4.5A) as well as to MB49, a murine bladder cancer cell line (Figure 4.5B), indicating that these cell lines express perlecan.

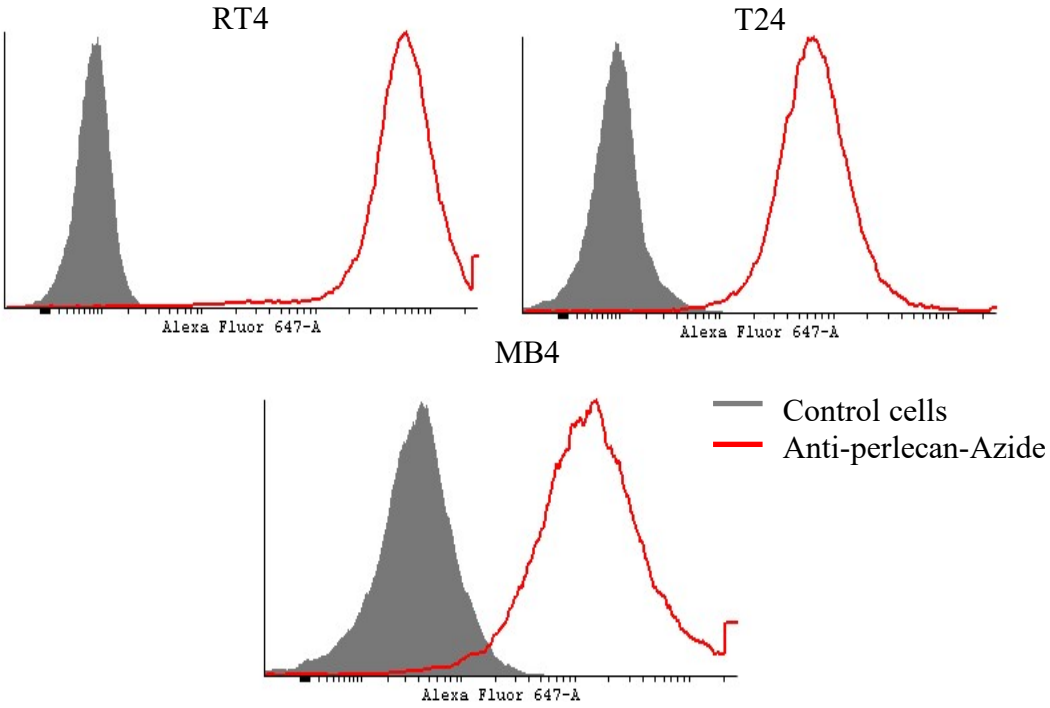

Figure 4.5: Binding of anti-perlecan-Az Ab to RT4 cells (A), T24 cells (B) and MB49 cells (C).

4.4.2.2 Cell uptake of antibody conjugated nanoparticles

Uptake of antibody-conjugated nanoparticles was studied in MB49 cells. Presence of antibody improved internalization of nanoparticles into cells (Figure 4.5). We saw a 2-fold

improvement in uptake of anti-perlecan-Az NP compared to control isotype IgG NP (P<0.05) and a 3-fold improvement in uptake of anti-perlecan-Az NP compared to control PEG NP (P<0.05)

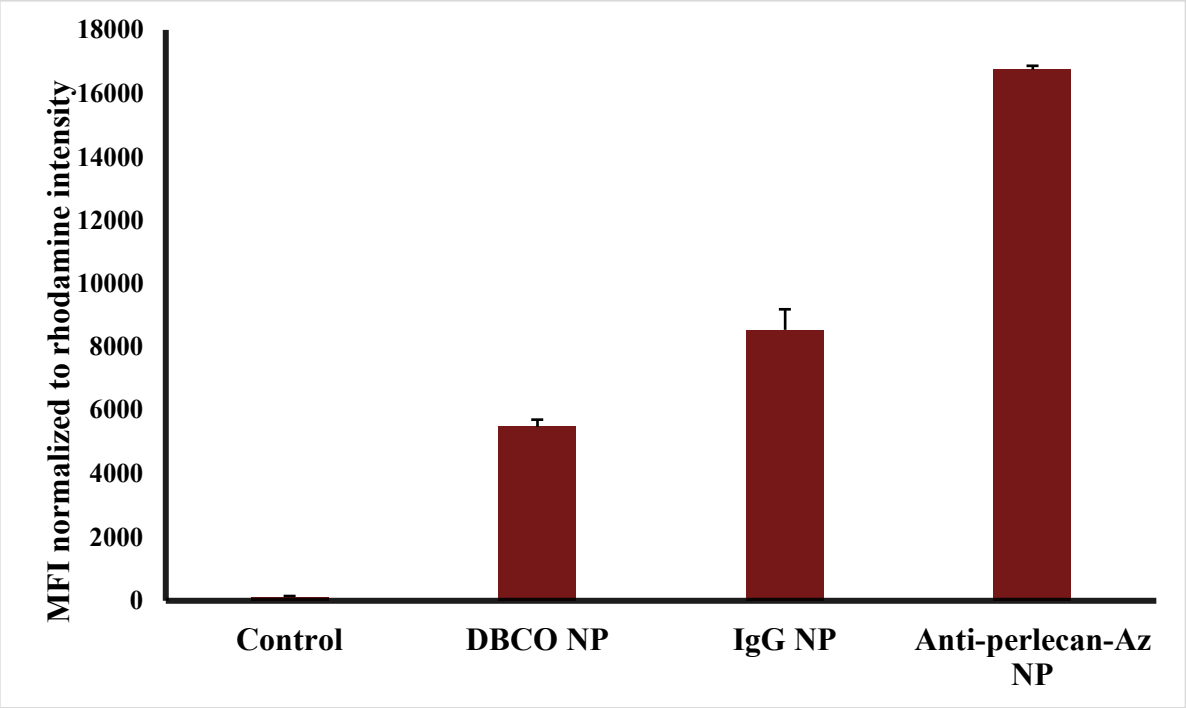

Figure 4.6: *In vitro* NP uptake with MB49 cells. Cells incubated with anti-perlecan-Az NP showed higher uptake (*P<0.05, two way ANOVA with multiple comparison tests, statistical significance is based off comparison between control cells, DBCO NP and IgG NP)

4.4.2.3 In vitro cytotoxicity with antibody conjugated nanoparticles

In order to test the potency of the antibody conjugated nanoparticles, we performed an *in vitro* cytotoxicity assay with MB49 cells. We observed that treatment with anti-perlecan-Az NP resulted in a significantly greater tumor cell kill as compared to the equivalent concentration of DBCO NP, IgG NP (31% viability as opposed to 62% and 51% in case of DBCO NP and IgG NP respectively) (P<0.05, two way ANOVA with multiple comparison tests, Figure 4.6).

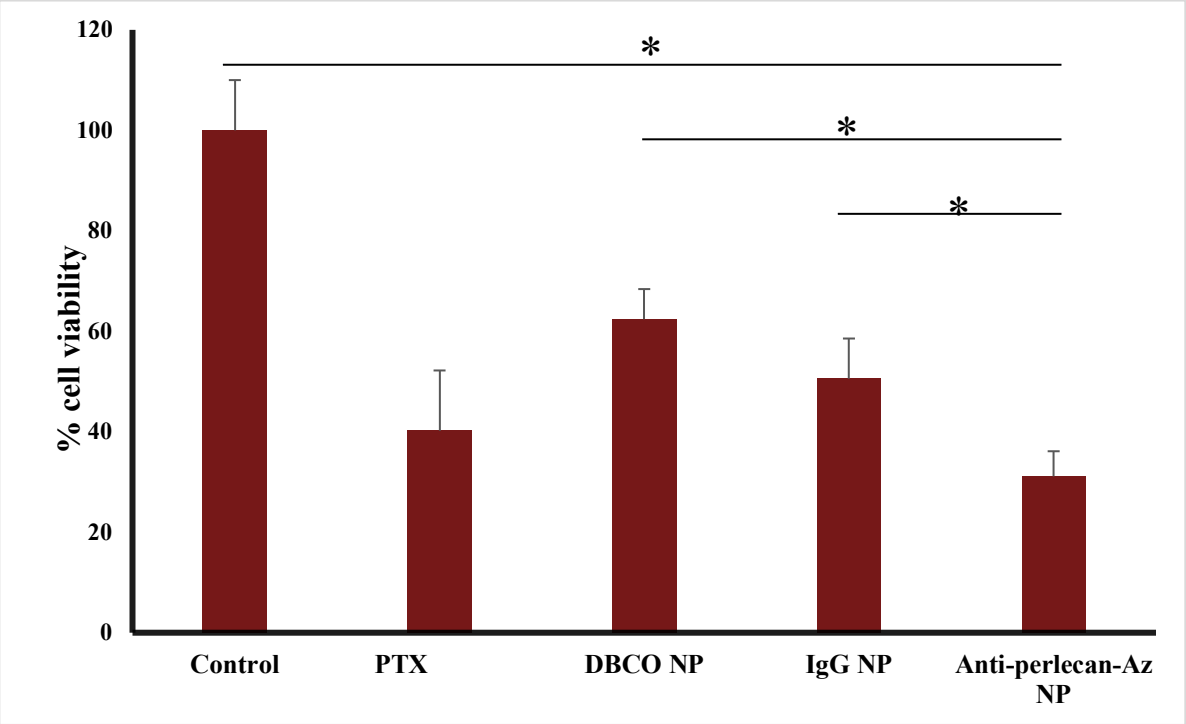

Figure 4.7: *In vitro* cytotoxicity study with MB49 cells. Anti-perlecan-Az NP treated groups showed higher cytotoxicity (*P<0.05, two way ANOVA with multiple comparison tests, statistical significance is based off comparison between control cells, PTX, DBCO NP and IgG NP)

4.4.2.4 Tumor growth inhibition with antibody conjugated nanoparticles

In order to determine the ability of antibody conjugated nanoparticles to improve drug delivery *in vivo*, we tested the efficacy in the MB49 orthotopic non-muscle invasive mouse bladder tumor model (Figure 4.7). Previous studies have shown that intra-tumoral administration of the treatments leads to increased accumulation of the chemotherapeutic drug with minimal off target effects [122–125]. So, we compared our formulations via two routes of administration, tail vein injection (IV) and directly into the bladder via urethral catheter (IT). We observed complete tumor growth inhibition with AM6-Az NP given via IT route (P<0.001, statistical significance is based on comparison between untreated and IgG NP via IT on the last day of the study). Interestingly,

we observed improved tumor growth inhibition with AM6-Az NP given via IV route as well ($P<0.001$, untreated and IgG NP via IT and IV on the last day of the study).

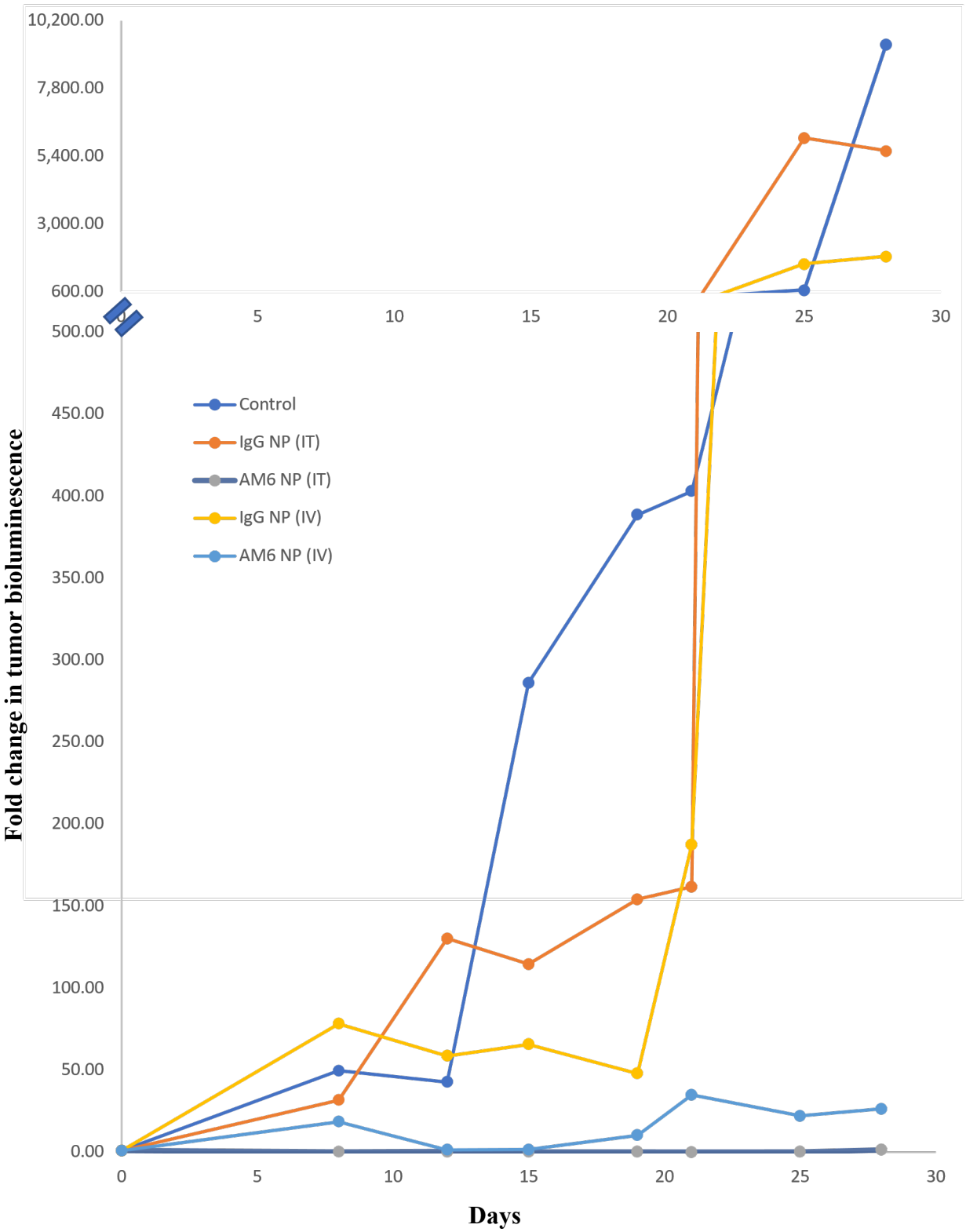

Figure 4.8: Efficacy study in C57/bl6 mice. 40 mg/kg AM6-Az NP administered via urethral catheter directly into the bladder showed complete tumor inhibition over IgG NP given via similar

route (**P<0.001, two-way ANOVA with multiple comparisons, statistical significance is based on comparison between untreated and IgG NP via IT on the last day of the study). 40 mg/kg AM6Az NP administered via tail vein injection showed significantly enhanced tumor inhibition over IgG NP given via similar route (**P<0.001, two-way ANOVA with multiple comparisons, statistical significance is based on comparison between untreated and IgG NP via IT on the last day of the study).

4.4.2.5 Ex vivo immunohistological analysis of tumors

In addition to monitoring tumor growth, we examined tumor sections from the efficacy study for cell proliferation (Ki-67) and apoptosis (cleaved caspase 3) (Figure 4.8). The frequency of Ki-67 positive cells was significantly ($p < 0.05$) higher in tumor sections from control group, IgG NP (IT) and IgG NP (IV) than that in AM6 NP (IT) and AM6 NP (IV) groups. Lowest cell proliferation was observed in sections from tumors treated with AM6 NP administered via urethral catheter. Further, there was an increase in the number of apoptotic cells in AM6 NP treated tumors (administered via urethral catheter and tail vein injection) than that in control and IgG NP treatment groups.

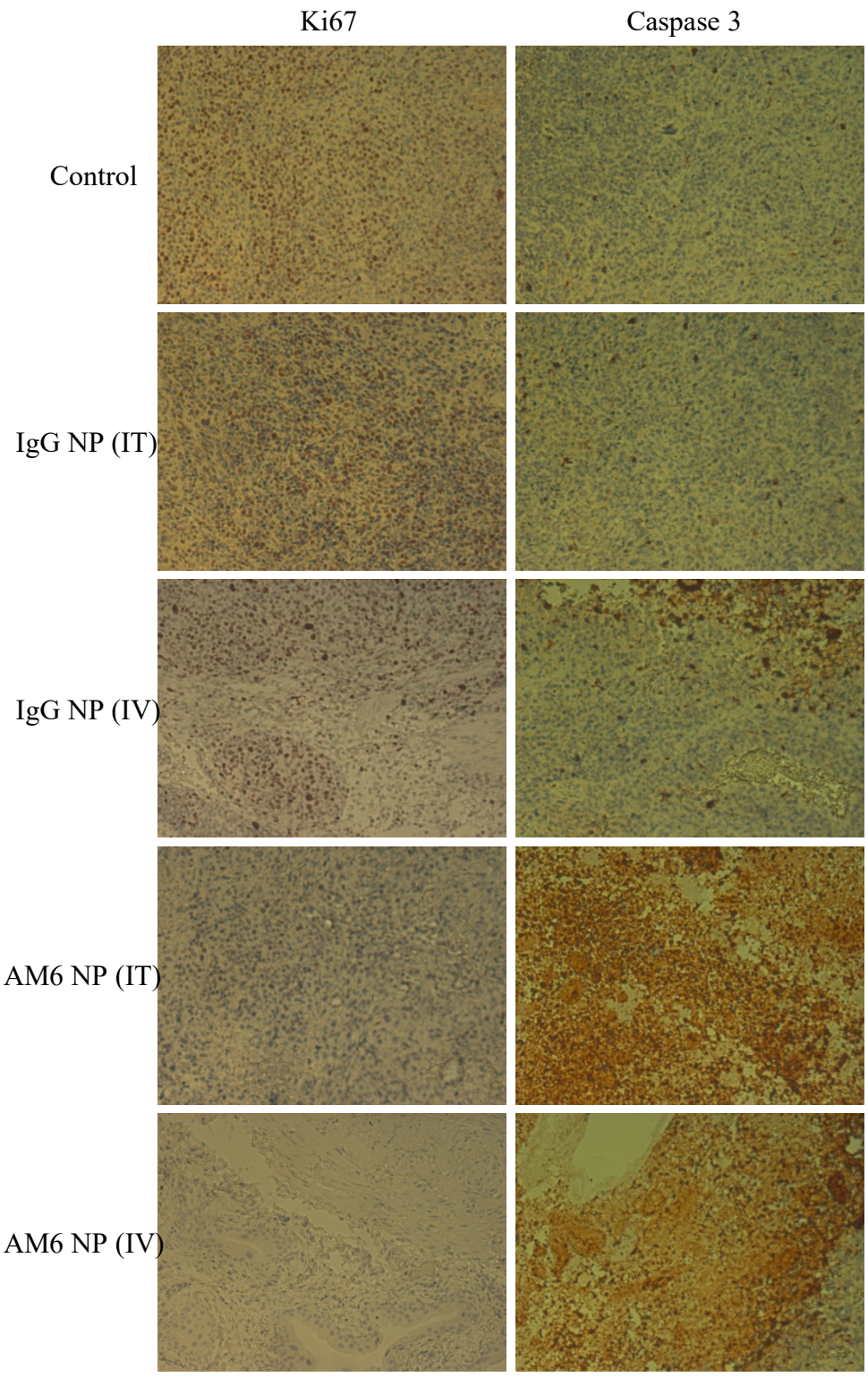
Ki67
Caspase 3
Control
IgG NP (IT)
IgG NP (IV)
AM6 NP (IT)
AM6 NP (IV)

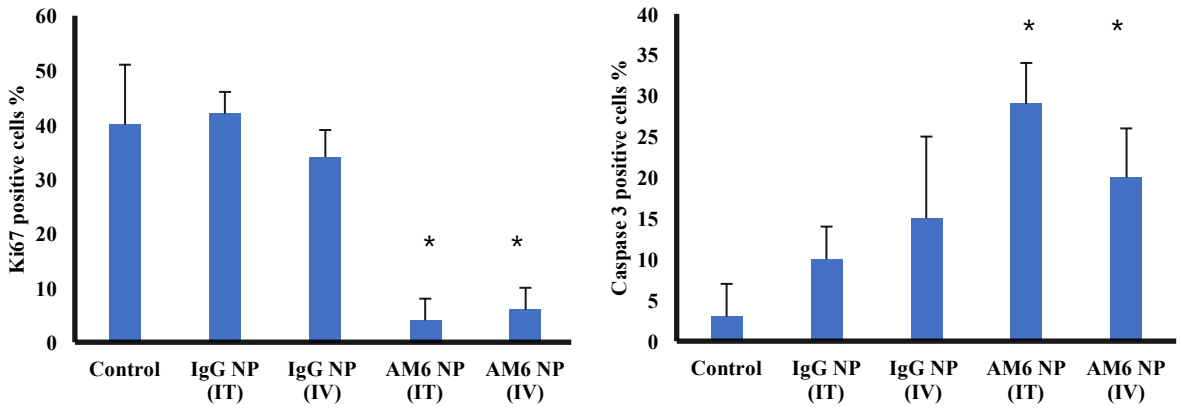

Figure 4.9 *Ex vivo* IHC analysis of bladder cancer tumor collected from efficacy study. **(A)** Representative images presented from each group. **(B)** Quantified data for percentage Ki67 positive cells. **(C)** Quantified data for percentage caspase 3 positive cells. *P<0.05, ordinary one-way ANOVA with multiple comparisons compared to control, IgG NP (IT) and IgG NP (IV).

4.4.2.6 Higher PTX accumulation in bladder with urethral catheterization route

We determined the bladder tumor accumulation of AM6 NP and IgG NP, each formulation containing PTX (Figure 4.9). The treatments were administered either via intravenous (IV) or directly into the bladder via urethral catheter (IT). Treatment with AM6 NP formulations administered via IT route led to higher bladder concentration than IgG NP given via the same route. In the mice where IgG NP administered via IT route, the PTX concentration in bladder decreased with time. Treatment with AM6 NP formulations administered via IV route led to higher bladder concentration over time compared to that with IgG NP given via similar route.

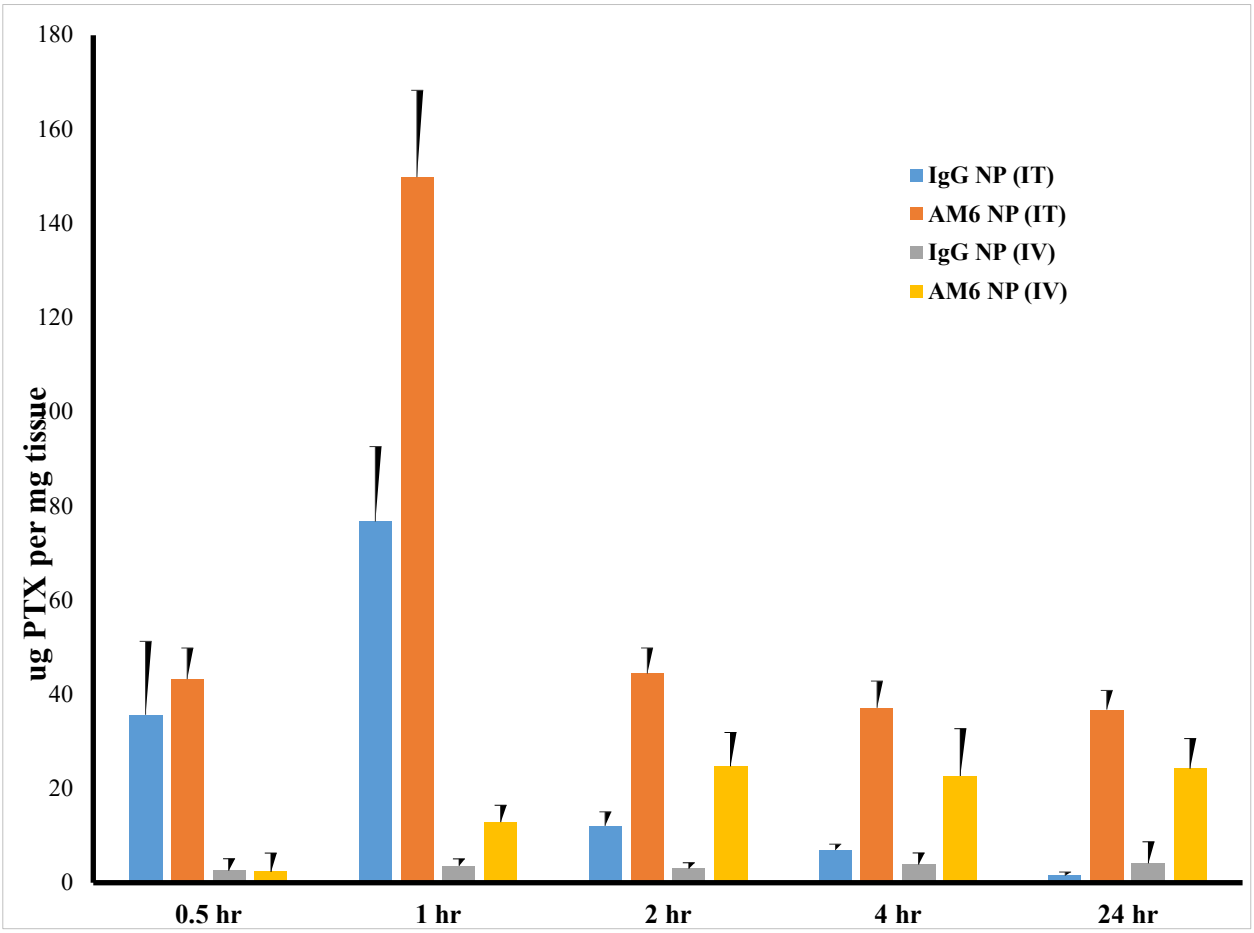

Figure 4.10: Bladder tumor accumulation of PTX.

4.5 Discussion

Conjugation of nanoparticles with antibodies combines the properties of nanoparticles with the specific and selective recognition ability of antibodies to antigens [3]. Also, the improvements in cellular delivery as well as intracellular stability are two additional advantages of using antibody conjugated nanoparticles [126].

PLGA was chosen as the polymer of choice due to one primary reason – the degradation products i.e. lactic acid and glycolic acid are naturally found in the body and thus toxicity

from the excipients would be minimal [127]. A number of other groups have used PLGA nanoparticles for cancer nanotherapy with minimal toxicity issues [82,128]. The nanoparticles were grafted on the surface with the block co-polymer PLA-PEG-DBCO using IAASF technique [86]. The DBCO group served as the reactive functional group on the nanoparticle surface for the conjugation of glycoengineered antibody by click chemistry. Characterization of the antibody-nanoparticle conjugates revealed a stable bond between the antibody and nanoparticles. The physical characteristics of nanoparticles were not significantly affected by presence of the antibody, likely due to the small number of antibody molecules conjugated to nanoparticles.

Breast cancer takes the lead in the National Cancer Institute's (NCI) database on funding for different types of cancer from 2007 through 2013 [129]. Close to $600,000,000 has been spent on breast cancer research each year [130]. This has resulted in improved diagnosis and advanced therapeutics, which, in turn, have significantly improved the survival rates of breast cancer. However, TNBC patients still have only a few treatment options available to them. In addition, most patients develop resistance to these therapies.

Bladder cancer is the second most common cancer of the urogenital tract with nearly 81,000 new cases and 20,000 deaths expected in 2018 [131] . High rates of recurrence require lifelong follow-up, which makes bladder cancer one of the costliest cancers to treat. Bladder cancer that has invaded the muscle layer may metastasize to liver, lung or bone via the lymphatic system. Multimodal therapy of advanced tumors results in only 20-40% survival after 5 years [131]. Therefore, effective treatment strategies aimed at reducing the recurrence and

progression of superficial bladder cancer as well as improving therapeutic outcome in patients with advanced disease are urgently needed.

Using phage display, our laboratory has successfully developed anti-perlecan antibody (AM6) [120]. It has also been shown that, high perlecan expression correlates with significantly poorer survival in TNBC and bladder cancer[120]. So, anti-perlecan antibody conjugated nanoparticles were used for targeting TNBC and bladder cancer. We observed a 2-3 fold improvement in cell uptake with AM6 NPs in both TNBC and bladder cancer cell lines. There was a significant improvement in the *in vitro* cytotoxicity of paclitaxel when delivered using AM6 NPs in both TNBC and bladder cancer cell lines, that can likely be attributed to both increased cellular uptake and longer retention of targeted NPs, resulting in higher drug concentrations inside the cell.

I*n vivo* studies in a subcutaneous model of TNBC showed significantly improved tumor growth inhibition *in vivo* with AM6 NPs relative to nontargeted isotype IgG NPs. Our observation of targeted NPs showing improved therapeutic efficacy is similar to previous reports [118,129,132]. However, in the non-muscle invasive bladder cancer model, we observed complete tumor growth inhibition with AM6-Az NP given through the urethral catheter and improved tumor growth inhibition with AM6-Az NP given via tail vein relative to nontargeted isotype IgG NPs given via both the routes. This data correlates with the higher PTX concentrations observed in bladder with AM6-Az NP given through the urethral catheter. Also, the PTX bladder concentration in mice administered with IgG NP via urethral catheter also decreased over time indicating that nanoparticles conjugated to nonspecific antibody may not be binding to the tumor cells on the bladder wall. Increase in the PTX concentration with AM6-Az

NP is likely due to the binding of the anti-perlecan antibody to perlecan expressed on the tumor cells. These results thus indicate that administering NPs directly into the bladder improves antitumor efficacy, which is similar to the previous reports that show improved tumor growth inhibition following local delivery of nanomedicine [77,122,123,133]. It is interesting to note that the IV delivery results in significant tumor growth inhibition (albeit less than that following the intravesical route). This may be because of effective targeting of NPs to the bladder tumor following IV delivery. It will be interesting to determine differences in toxicity and side effects (arising from non-specific distribution of PTX) between the IV and IT route.

4.6 Conclusion

Glycoengineered AM6 antibody was used to generate perlecan-targeted nanoparticles loaded with paclitaxel. These antibody conjugated nanoparticles showed enhanced antitumor efficacy in vitro as well as in vivo in TNBC models. Targeted nanoparticles also demonstrated enhanced antitumor efficacy in vitro and complete tumor growth inhibition in vivo in a non-muscle invasive bladder cancer model.

Chapter 5: Summary

The central objective of this thesis was to advance a new antibody glycoengineering technology that will allow for facile synthesis of antibody-based drug delivery systems. In order to accomplish this objective, we expressed antibodies with artificial azide groups using a novel glycoengineering strategy. This strategy involved incorporation of azido sugars in the N-glycan region of anti-perlecan and anti-CD133 antibodies. The results indicated that glycoengineering strategy can be used for different production systems and for different antibodies. Further, cyclooctyne containing payloads including fluorophores and PEG conjugates were successfully conjugated to glycoengineered antibodies using click chemistry. Upon quantification we found that we were able to incorporate 2-3 azide molecules per antibody. Our studies showed that incorporation of azido sugars and subsequent click reaction did not affect the antigen binding or in vivo tumor accumulation of the antibody. In future, the number of azide groups introduced per antibody can be further increased by completely depleting the natural sugars in the media during the production of the antibody and substituting it with non-natural sugars containing azide.

Antibodies in the clinic have been utilized for versatile applications including, but not limited to, antibody-drug conjugates, diagnostic agents, targeting ligands and as therapeutics themselves. In chapters 3 and 4, we developed two different types of antibody conjugates viz., antibody drug conjugate (ADC) and antibody conjugated nanoparticles for therapeutic applications using the glycoengineered antibody.

In chapter 3, our strategy for site-specific antibody drug conjugation technology involved coupling drug molecules to modified N-glycans on the antibody. The ADC with glycoengineered anti-perlecan antibody, DBCO-PEG as the linker and monomethyl auristatin

E as the drug had 2-3 drug molecules per antibody. This ADC enhanced antitumor efficacy in vitro as well as in vivo. We also performed internalization studies with anti-perlecan antibody, which suggested that it is slowly internalized into tumor cells. This suggests that using cleavable linker technology in the ADC could further improve its anticancer effectiveness in future.

In chapter 4, glycoengineered anti-perlecan antibody was used to generate antibody conjugated nanoparticles. PTX loaded PLGA nanoparticles were surface functionalized with PLA-PEG DBCO using a previously developed technique in lab. The DBCO group served as the reactive functional group on the nanoparticle surface for conjugation of glycoengineered antibody via click chemistry. We were able to achieve a stable bond between the antibody and nanoparticles without affecting the physical characteristics of nanoparticles or the antigen affinity of antibody. These antibody conjugated nanoparticles showed enhanced antitumor efficacy in vitro as well as in vivo in TNBC models. These targeted nanoparticles also demonstrated enhanced antitumor efficacy in vitro and complete tumor growth inhibition in vivo in a non-muscle invasive bladder cancer model.

In conclusion, our studies show that the antibody glycoengineering strategy advanced here is an effective approach for incorporating drug payload in the antibody, and can therefore be expected have a significant impact on antibody-based therapeutics.

Bibliography

1. Adams GP, Weiner LM. Monoclonal antibody therapy of cancer. *Nat Biotechnol*.

2005;23(9):1147-1157. doi:10.1038/nbt1137

2. Smolen JS, Aletaha D. Rheumatoid arthritis therapy reappraisal: Strategies, opportunities and challenges. *Nat Rev Rheumatol*. 2015;11(5):276-289. doi:10.1038/nrrheum.2015.8

3. Arruebo M, Valladares M, González-Fernández Á. Antibody-conjugated nanoparticles for biomedical applications. *J Nanomater*. 2009;2009. doi:10.1155/2009/439389

4. Flemming A. Fine-tuning antibody–drug conjugates. *Nat Rev Drug Discov*.

2014;13(3):178. doi:10.1038/nrd4266

5. Schreiber RD, Old LJ, Smyth MJ. Cancer immunoediting: integrating immunity's roles in cancer suppression and promotion. *Science*. 2011;331(6024):1565-1570. doi:10.1126/science.1203486

6. Farkona S, Diamandis EP, Blasutig IM. Cancer immunotherapy: The beginning of the end of cancer? *BMC Med*. 2016;14(1):1-18. doi:10.1186/s12916-016-0623-5

7. Jefferis R. CCE IX : Review Glycosylation of Recombinant Antibody Therapeutics.

Society. 2005:11-16.

8. Ecker DM, Jones SD, Levine HL. The therapeutic monoclonal antibody market. *MAbs*.

2015;7(1):9-14. doi:10.4161/19420862.2015.989042

9. Lobo ED, Hansen RJ, Balthasar JP. Antibody pharmacokinetics and pharmacodynamics. *J*

Pharm Sci. 2004;93(11):2645-2668. doi:10.1002/jps.20178

10. Lucas A, Price L, Schorzman A, et al. Factors Affecting the Pharmacology of Antibody–

Drug Conjugates. *Antibodies*. 2018;7(1):10. doi:10.3390/antib7010010

11. Otagiri M, Giam Chuang VT, Immunobiology, Murphy K, Weaver C. *Janeway ' S 9 Th*

Edition.; 2017. doi:10.1007/978-981-10-2116-9

12. Rayner LE, Hui GK, Gor J, Heenan RK, Dalby PA, Perkins SJ. The solution structures of two human IgG1 antibodies show conformational stability and accommodate their C1q and FcγR ligands. *J Biol Chem*. 2015;290(13):8420-8438. doi:10.1074/jbc.M114.631002
13. Lambert JM, Morris CQ. Antibody–Drug Conjugates (ADCs) for Personalized Treatment of Solid Tumors: A Review. *Adv Ther*. 2017;34(5):1015-1035. doi:10.1007/s12325-017-
0519-6

14. Uzman A. Molecular biology of the cell (4th ed.): Alberts, B., Johnson, A., Lewis, J.,

Raff, M., Roberts, K., and Walter, P. *Biochem Mol Biol Educ*. 2003;31(4):212-214. doi:doi:10.1002/bmb.2003.494031049999
15. Milstein C, Alerts E. Pillars Article : Continuous cultures of fused cells secreting antibody of predefined. *Nature*. 1975;256(5517):495-497.
16. Issa F. Remote control of therapeutic T cells through a small molecule-gated chimeric receptor. *Transplantation*. 2015;99(12):2434. doi:10.1097/TP.0000000000001016
17. Pirofski L, Casadevall A, Rodriguez L, Zuckier LS, Scharff MD. Current state of the hybridoma technology. *J Clin Immunol*. 1990;10(6 Supplement). doi:10.1007/BF00918686
18. Brekke OH, Sandlie I. Therapeutic antibodies for human diseases at the dawn of the twenty-first century. *Nat Rev Drug Discov*. 2003;2(1):52-62. doi:10.1038/nrd984
19. Smith SL. Ten Years of Orthoclone OKT3 (Muromonab-CD3): A Review. *J Transpl*

Coord. 1996;6(3):109-121. doi:10.1177/090591999600600304

20. Harding FA, Stickler MM, Razo J, DuBridge RB. The immunogenicity of humanized and fully human antibodies: Residual immunogenicity resides in the CDR regions. *MAbs*.

2010;2(3):256-265. doi:10.4161/mabs.2.3.11641

21. Wang Q, Chung CY, Chough S, Betenbaugh MJ. Antibody glycoengineering strategies in mammalian cells. *Biotechnol Bioeng*. 2018;115(6):1378-1393. doi:10.1002/bit.26567
22. Cho K, Wang X, Nie S, Chen Z, Shin DM. Therapeutic nanoparticles for drug delivery in cancer. *Clin Cancer Res*. 2008;14(5):1310-1316. doi:10.1158/1078-0432.CCR-07-1441
23. Tonelli AR, Lottenberg R, Allan RW, Sriram PS. Rituximab-induced hypersensitivity pneumonitis. *Respiration*. 2009;78(2):225-229. doi:10.1159/000163069
24. The official website of the Nobel Prize - NobelPrize.org. https://www.nobelprize.org/.

Accessed December 4, 2019.

25. Humira | AbbVie. https://www.abbvie.com/our-science/pipeline/humira.html. Accessed

December 4, 2019.

26. Nixon AE, Sexton DJ, Ladner RC. Drugs derived from phage display from candidate identification to clinical practice. *MAbs*. 2014;6(1):73-85. doi:10.4161/mabs.27240
27. Urquhart L. Top drugs and companies by sales in 2018. *Nat Rev Drug Discov*. March

2019. doi:10.1038/d41573-019-00049-0

28. Bazan J, Całkosiñski I, Gamian A. Phage displaya powerful technique for immunotherapy: 1. Introduction and potential of therapeutic applications. *Hum Vaccines Immunother*. 2012;8(12):1817-1828. doi:10.4161/hv.21703

29. Wang L, Amphlett G, Blättler WA, Lambert JM, Zhang W. Structural characterization of the maytansinoid-monoclonal antibody immunoconjugate, huN901-DM1, by mass spectrometry. *Protein Sci*. 2005;14(9):2436-2446. doi:10.1110/ps.051478705
30. Strohl WR. Current progress in innovative engineered antibodies. *Protein Cell*. 2018;9(1):86-120. doi:10.1007/s13238-017-0457-8

31. Kanyavuz A, Marey-Jarossay A, Lacroix-Desmazes S, Dimitrov JD. Breaking the law:

unconventional strategies for antibody diversification. *Nat Rev Immunol*. 2019;19(6):355-

368. doi:10.1038/s41577-019-0126-7

32. Liu L. Antibody glycosylation and its impact on the pharmacokinetics and pharmacodynamics of monoclonal antibodies and Fc-fusion proteins. *J Pharm Sci*. 2015;104(6):1866-1884. doi:10.1002/jps.24444

33. Stefanich EG, Ren S, Danilenko DM, et al. Evidence for an asialoglycoprotein receptor on nonparenchymal cells for O-linked glycoproteins. *J Pharmacol Exp Ther*. 2008;327(2):308-315. doi:10.1124/jpet.108.142232

34. Pennica D, Lam VT, Weber RF, et al. Biochemical characterization of the extracellular domain of the 75-kilodalton tumor necrosis factor receptor. *Biochemistry*. 1993;32(12):3131-3138. doi:10.1021/bi00063a027

35. Arnold JN, Wormald MR, Sim RB, Rudd PM, Dwek RA. The Impact of Glycosylation on the Biological Function and Structure of Human Immunoglobulins. *Annu Rev Immunol*. 2007;25(1):21-50. doi:10.1146/annurev.immunol.25.022106.141702
36. Krapp S, Mimura Y, Jefferis R, Huber R, Sondermann P. Structural Analysis of Human

IgG-Fc Glycoforms Reveals a Correlation Between Glycosylation and Structural Integrity.

J Mol Biol. 2003;325(5):979-989. doi:10.1016/S0022-2836(02)01250-0

37. Jefferis R. Isotype and glycoform selection for antibody therapeutics. *Arch Biochem*

Biophys. 2012;526(2):159-166. doi:10.1016/J.ABB.2012.03.021

38. Hayes JM, Cosgrave EFJ, Struwe WB, et al. Glycosylation and Fc receptors. *Curr Top*

Microbiol Immunol. 2014;382:165-199. doi:10.1007/978-3-319-07911-0_8

39. Kornfeld R, Kornfeld S. Assembly of asparagine-linked oligosaccharides. *Annu Rev*

Biochem. 1985;54:631-664. doi:10.1146/annurev.bi.54.070185.003215

40. Kornfeld R, Kornfeld S. Comparative aspects of glycoprotein structure. *Annu Rev*

Biochem. 1976;45:217-237. doi:10.1146/annurev.bi.45.070176.001245

41. Kornfeld R, Keller J, Baenziger J, Kornfeld S. The structure of the glycopeptide of human gamma G myeloma proteins. *J Biol Chem*. 1971;246(10):3259-3268.
42. Kolb HC, Sharpless KB. The growing impact of click chemistry on drug discovery. *Drug*

Discov Today. 2003;8(24):1128-1137. doi:10.1016/S1359-6446(03)02933-7

43. Agard NJ, Prescher JA, Bertozzi CR. A Strain-Promoted [3 + 2] Azide−Alkyne Cycloaddition for Covalent Modification of Biomolecules in Living Systems. *J Am Chem Soc*. 2004;126(46):15046-15047. doi:10.1021/ja044996f

44. Tornøe CW, Christensen C, Meldal M. Peptidotriazoles on Solid Phase: [1,2,3]-Triazoles by Regiospecific Copper(I)-Catalyzed 1,3-Dipolar Cycloadditions of Terminal Alkynes to
Azides. *J Org Chem*. 2002;67(9):3057-3064. doi:10.1021/jo011148j

45. Rostovtsev V V., Green LG, Fokin V V., Sharpless KB. A Stepwise Huisgen Cycloaddition Process: Copper(I)-Catalyzed Regioselective “Ligation” of Azides and Terminal Alkynes. *Angew Chemie Int Ed*. 2002;41(14):2596-2599. doi:10.1002/1521-3773(20020715)41:14<2596::AID-ANIE2596>3.0.CO;2-4

46. Of H, Information P. Reference ID : 3662552 DESCRIPTION Reference ID : 3662552.

2011;(2).

47. See full prescribing information for complete boxed warning •. 2019.

48. FULL PRESCRIBING INFORMATION WARNING : HEPATOTOXICITY

Hepatotoxicity , including severe or fatal hepatic veno-occlusive disease (VOD), also

known as sinusoidal obstruction syndrome (SOS), has been reported in association with the use of MYLOTARG as a . 2000:1-19.

49. Reference ID : 4140675 Reference ID : 4140675. 2017:1-26.

50. FULL PRESCRIBING INFORMATION WARNING : CAPILLARY LEAK SYNDROME and HEMOLYTIC UREMIC SYNDROME Capillary Leak Syndrome (CLS), including life-threatening cases , occurred in patients receiving LUMOXITI .

Monitor weight and blood pressure ; check labs , i. 2018:1-25.

51. INDICATIONS AND USAGE POLIVY in combination with bendamustine and a

rituximab product is indicated for the treatment of adult patients with relapsed or refractory diffuse large B-cell lymphoma (DLBCL), not otherwise specified , after at least two prior . 2019.

52. Ducry L, Stump B. Antibody-drug conjugates: linking cytotoxic payloads to monoclonal antibodies. *Bioconjug Chem*. 2010;21(1):5-13. doi:10.1021/bc9002019

53. Sievers EL, Senter PD. Antibody-drug conjugates in cancer therapy. *Annu Rev Med*.

2013;64:15-29. doi:10.1146/annurev-med-050311-201823

54. Nolting B. Linker technologies for antibody-drug conjugates. *Methods Mol Biol*.

2013;1045:71-100. doi:10.1007/978-1-62703-541-5_5

55. Bareford LM, Swaan PW. Endocytic mechanisms for targeted drug delivery. *Adv Drug*

Deliv Rev. 2007;59(8):748-758. doi:10.1016/j.addr.2007.06.008

56. Roopenian DC, Akilesh S. FcRn: the neonatal Fc receptor comes of age. *Nat Rev*

Immunol. 2007;7(9):715-725. doi:10.1038/nri2155

57. Ritchie M, Tchistiakova L, Scott N. Implications of receptor-mediated endocytosis and intracellular trafficking dynamics in the development of antibody drug conjugates. *MAbs*. 2013;5(1):13-21. doi:10.4161/mabs.22854

58. Chari RVJ. Targeted cancer therapy: conferring specificity to cytotoxic drugs. *Acc Chem*

Res. 2008;41(1):98-107. doi:10.1021/ar700108g

59. Teicher BA, Chari RVJ. Antibody conjugate therapeutics: challenges and potential. *Clin*

Cancer Res. 2011;17(20):6389-6397. doi:10.1158/1078-0432.CCR-11-1417

60. Chari RVJ, Miller ML, Widdison WC. Antibody-drug conjugates: an emerging concept in cancer therapy. *Angew Chem Int Ed Engl*. 2014;53(15):3796-3827. doi:10.1002/anie.201307628

61. Senter PD, Sievers EL. The discovery and development of brentuximab vedotin for use in relapsed Hodgkin lymphoma and systemic anaplastic large cell lymphoma. *Nat Biotechnol*. 2012;30(7):631-637. doi:10.1038/nbt.2289

62. Lambert JM, Chari RVJ. Ado-trastuzumab Emtansine (T-DM1): an antibody-drug conjugate (ADC) for HER2-positive breast cancer. *J Med Chem*. 2014;57(16):6949-6964. doi:10.1021/jm500766w

63. Smith AL, Nicolaou KC. The enediyne antibiotics. *J Med Chem*. 1996;39(11):2103-2117. doi:10.1021/jm9600398

64. Pettit GR, Kamano Y, Herald CL, et al. The isolation and structure of a remarkable marine animal antineoplastic constituent: dolastatin 10. *J Am Chem Soc*. 1987;109(22):6883-
6885. doi:10.1021/ja00256a070

65. Widdison WC, Wilhelm SD, Cavanagh EE, et al. Semisynthetic maytansine analogues for the targeted treatment of cancer. *J Med Chem*. 2006;49(14):4392-4408. doi:10.1021/jm060319f

66. Kupchan SM, Sneden AT, Branfman AR, et al. Structural requirements for antileukemic activity among the naturally occurring and semisynthetic maytansinoids. *J Med Chem*.

1978;21(1):31-37. doi:10.1021/jm00199a006

67. Singh R, Lambert JM, Chari RVJ. Antibody-Drug Conjugates: New Frontier in Cancer

Therapeutics. *Handb Ther Antibodies*. September 2014:341-362. doi:doi:10.1002/9783527682423.ch13
68. Singh R, Setiady YY, Ponte J, et al. A New Triglycyl Peptide Linker for Antibody-Drug

Conjugates (ADCs) with Improved Targeted Killing of Cancer Cells. *Mol Cancer Ther*.

2016;15(6):1311-1320. doi:10.1158/1535-7163.MCT-16-0021

69. Erickson HK, Widdison WC, Mayo MF, et al. Tumor delivery and in vivo processing of disulfide-linked and thioether-linked antibody-maytansinoid conjugates. *Bioconjug Chem*.
2010;21(1):84-92. doi:10.1021/bc900315y

70. Erickson HK, Park PU, Widdison WC, et al. Antibody-maytansinoid conjugates are activated in targeted cancer cells by lysosomal degradation and linker-dependent intracellular processing. *Cancer Res*. 2006;66(8):4426-4433. doi:10.1158/0008-5472.CAN-05-4489

71. Erickson HK, Lambert JM. ADME of antibody-maytansinoid conjugates. *AAPS J*.

2012;14(4):799-805. doi:10.1208/s12248-012-9386-x

72. Sharkey RM, Goldenberg DM. Use of antibodies and immunoconjugates for the therapy of more accessible cancers. *Adv Drug Deliv Rev*. 2008;60(12):1407-1420. doi:10.1016/j.addr.2008.04.011
73. Desai MP, Labhasetwar V, Walter E, Levy RJ, Amidon GL. The mechanism of uptake of biodegradable microparticles in Caco-2 cells is size dependent. *Pharm Res*.
1997;14(11):1568-1573. doi:10.1023/a:1012126301290

74. Peer D, Karp JM, Hong S, Farokhzad OC, Margalit R, Langer R. Nanocarriers as an emerging platform for cancer therapy. *Nat Nanotechnol*. 2007;2(12):751-760. doi:10.1038/nnano.2007.387

75. Hashizume H, Baluk P, Morikawa S, et al. Openings between defective endothelial cells explain tumor vessel leakiness. *Am J Pathol*. 2000;156(4):1363-1380. doi:10.1016/S00029440(10)65006-7
76. Leu AJ, Berk DA, Lymboussaki A, Alitalo K, Jain RK. Absence of functional lymphatics within a murine sarcoma: a molecular and functional evaluation. *Cancer Res*.
2000;60(16):4324-4327.

77. Torchilin V. Tumor delivery of macromolecular drugs based on the EPR effect. *Adv Drug*

Deliv Rev. 2011;63(3):131-135. doi:10.1016/j.addr.2010.03.011

78. Does nanomedicine have a delivery problem? | June 20, 2016 Issue - Vol. 94 Issue 25 | Chemical & Engineering News. https://cen.acs.org/articles/94/i25/Does-nanomedicinedelivery-problem.html. Accessed December 8, 2019.
79. Bartlett DW, Su H, Hildebrandt IJ, Weber WA, Davis ME. Impact of tumor-specific targeting on the biodistribution and efficacy of siRNA nanoparticles measured by multimodality in vivo imaging. *Proc Natl Acad Sci U S A*. 2007;104(39):15549-15554. doi:10.1073/pnas.0707461104
80. Kirpotin DB, Drummond DC, Shao Y, et al. Antibody targeting of long-circulating lipidic nanoparticles does not increase tumor localization but does increase internalization in animal models. *Cancer Res*. 2006;66(13):6732-6740. doi:10.1158/0008-5472.CAN-05-4199

81. Xu Y, Kim C-S, Saylor DM, Koo D. Polymer degradation and drug delivery in PLGAbased drug-polymer applications: A review of experiments and theories. *J Biomed Mater*

Res B Appl Biomater. 2017;105(6):1692-1716. doi:10.1002/jbm.b.33648

82. Panyam J, Labhasetwar V. Biodegradable nanoparticles for drug and gene delivery to cells and tissue. *Adv Drug Deliv Rev*. 2003;55(3):329-347. doi:10.1016/s0169-409x(02)00228-
4

83. Panyam J, Zhou W-Z, Prabha S, Sahoo SK, Labhasetwar V. Rapid endo-lysosomal escape of poly(DL-lactide-co-glycolide) nanoparticles: implications for drug and gene delivery.
FASEB J Off Publ Fed Am Soc Exp Biol. 2002;16(10):1217-1226. doi:10.1096/fj.02-

0088com

84. Owens DE 3rd, Peppas NA. Opsonization, biodistribution, and pharmacokinetics of polymeric nanoparticles. *Int J Pharm*. 2006;307(1):93-102. doi:10.1016/j.ijpharm.2005.10.010
85. Harris JM, Chess RB. Effect of pegylation on pharmaceuticals. *Nat Rev Drug Discov*.

2003;2(3):214-221. doi:10.1038/nrd1033

86. Patil YB, Toti US, Khdair A, Ma L, Panyam J. Single-step surface functionalization of polymeric nanoparticles for targeted drug delivery. *Biomaterials*. 2009;30(5):859-866. doi:10.1016/J.BIOMATERIALS.2008.09.056
87. Nejadmoghaddam M, Minai-tehrani A, Ghahremanzadeh R. Antibody-Drug Conjugates :

Possibilities and Challenges. 2019;11(1).

88. Dhakal D, Dhakal Y, Sohng JK. Book Review : Antibody-Drug Conjugates :

Fundamentals , Drug Development , and Clinical Outcomes to Target Cancer.

2017;8(October):3-5. doi:10.1021/bc5004982

89. Vidarsson G, Dekkers G, Rispens T. IgG subclasses and allotypes: From structure to effector functions. *Front Immunol*. 2014;5(OCT). doi:10.3389/fimmu.2014.00520

90. Strop P, Liu SH, Dorywalska M, et al. Location matters: Site of conjugation modulates stability and pharmacokinetics of antibody drug conjugates. *Chem Biol*. 2013;20(2):161-
167. doi:10.1016/j.chembiol.2013.01.010

91. Yamada K, Ito Y. Recent Chemical Approaches for Site-Specific Conjugation of Native

Antibodies: Technologies toward Next-Generation Antibody–Drug Conjugates.

ChemBioChem. 2019:2729-2737. doi:10.1002/cbic.201900178

92. Van Geel R, Wijdeven MA, Heesbeen R, et al. Chemoenzymatic Conjugation of Toxic Payloads to the Globally Conserved N-Glycan of Native mAbs Provides Homogeneous and Highly Efficacious Antibody-Drug Conjugates. *Bioconjug Chem*. 2015;26(11):22332242. doi:10.1021/acs.bioconjchem.5b00224

93. O'Connor LJ, Mistry IN, Collins SL, et al. CYP450 Enzymes Effect Oxygen-Dependent

Reduction of Azide-Based Fluorogenic Dyes. *ACS Cent Sci*. 2017;3(1):20-30. doi:10.1021/acscentsci.6b00276

94. Swaminathan SK, Olin MR, Forster CL, Cruz KSS, Panyam J, Ohlfest JR. Identification of a novel monoclonal antibody recognizing CD133. *J Immunol Methods*. 2010;361(1-
2):110-115. doi:10.1016/J.JIM.2010.07.007

95. Toma A, Otsuji E, Kuriu Y, et al. Monoclonal antibody A7-superparamagnetic iron oxide as contrast agent of MR imaging of rectal carcinoma. *Br J Cancer*. 2005;93(1):131-136. doi:10.1038/sj.bjc.6602668

96. Takashima H, Tsuji AB, Saga T, et al. Molecular imaging using an anti-human tissue factor monoclonal antibody in an orthotopic glioma xenograft model. *Sci Rep*. 2017;7(1):4-9. doi:10.1038/s41598-017-12563-5

97. Ju M-S, Jung ST. Aglycosylated full-length IgG antibodies: steps toward next-generation immunotherapeutics. *Curr Opin Biotechnol*. 2014;30:128-139. doi:10.1016/J.COPBIO.2014.06.013

98. Acchione M, Kwon H, Jochheim CM, Atkins WM. Impact of linker and conjugation chemistry on antigen binding, Fc receptor binding and thermal stability of model antibody-drug conjugates. *MAbs*. 2012;4(3):362-372. doi:10.4161/mabs.19449
99. Ordás I, Mould DR, Feagan BG, Sandborn WJ. Anti-TNF monoclonal antibodies in inflammatory bowel disease: Pharmacokinetics-based dosing paradigms. *Clin Pharmacol Ther*. 2012;91(4):635-646. doi:10.1038/clpt.2011.328
100. Krop IE, Kim S-B, González-Martín A, et al. Trastuzumab emtansine versus treatment of physician's choice for pretreated HER2-positive advanced breast cancer (TH3RESA): a randomised, open-label, phase 3 trial. *Lancet Oncol*. 2014;15(7):689-699. doi:10.1016/S1470-2045(14)70178-0

101. Hurvitz SA, Dirix L, Kocsis J, et al. Phase II randomized study of trastuzumab emtansine versus trastuzumab plus docetaxel in patients with human epidermal growth factor receptor 2-positive metastatic breast cancer. *J Clin Oncol*. 2013;31(9):1157-1163. doi:10.1200/JCO.2012.44.9694
102. Gopal AK, Chen R, Smith SE, et al. Durable remissions in a pivotal phase 2 study of brentuximab vedotin in relapsed or refractory Hodgkin lymphoma. *Blood*. 2015;125(8):1236-1243. doi:10.1182/blood-2014-08-595801

103. Lewis Phillips GD, Li G, Dugger DL, et al. Targeting HER2-positive breast cancer with trastuzumab-DM1, an antibody-cytotoxic drug conjugate. *Cancer Res*. 2008;68(22):9280-
9290. doi:10.1158/0008-5472.CAN-08-1776

104. Francisco JA, Cerveny CG, Meyer DL, et al. cAC10-vcMMAE, an anti-CD30monomethyl auristatin E conjugate with potent and selective antitumor activity. *Blood*.
2003;102(4):1458-1465. doi:10.1182/blood-2003-01-0039

105. Lee B-C, Chalouni C, Doll S, et al. FRET Reagent Reveals the Intracellular Processing of

Peptide-Linked Antibody–Drug Conjugates. *Bioconjug Chem*. 2018;29(7):2468-2477. doi:10.1021/acs.bioconjchem.8b00362
106. Wakankar A, Chen Y, Gokarn Y, Jacobson FS. Analytical methods for physicochemical characterization of antibody drug conjugates. *MAbs*. 2011;3(2):164-175. doi:10.4161/mabs.3.2.14960

107. Hamblett KJ, Senter PD, Chace DF, et al. Effects of drug loading on the antitumor activity of a monoclonal antibody drug conjugate. *Clin Cancer Res*. 2004;10(20):7063-7070.
doi:10.1158/1078-0432.CCR-04-0789

108. Peters C, Brown S. Antibody-drug conjugates as novel anti-cancer chemotherapeutics.

Biosci Rep. 2015;35(4). doi:10.1042/BSR20150089

109. Hashida S, Imagawa M, Inoue S, Ruan KH, Ishikawa E. More useful maleimide compounds for the conjugation of Fab' to horseradish peroxidase through thiol groups in the hinge. *J Appl Biochem*. 1984;6(1-2):56-63.
110. Labhasetwar V, Song C, Levy RJ. Nanoparticle drug delivery system for restenosis. *Adv*

Drug Deliv Rev. 1997;24(1):63-85. doi:10.1016/S0169-409X(96)00483-8

111. Gelperina S, Kisich K, Iseman MD, Heifets L. The potential advantages of nanoparticle drug delivery systems in chemotherapy of tuberculosis. *Am J Respir Crit Care Med*.
2005;172(12):1487-1490. doi:10.1164/rccm.200504-613PP

112. Fang J, Nakamura H, Maeda H. The EPR effect: Unique features of tumor blood vessels for drug delivery, factors involved, and limitations and augmentation of the effect. *Adv*

Drug Deliv Rev. 2011;63(3):136-151. doi:10.1016/j.addr.2010.04.009

113. Roque MC, Franco MS, Vilela JMC, Andrade MS, Barros ALB de, Oliveira* EAL and

MC. Development of Long-Circulating and Fusogenic Liposomes Coencapsulating Paclitaxel and Doxorubicin in Synergistic Ratio for the Treatment of Breast Cancer. *Curr Drug Deliv*. 2019;16(9):829-838.

doi:http://dx.doi.org/10.2174/1567201816666191016112717

114. Micha JP, Goldstein BH, Birk CL, Rettenmaier MA, Brown J V. Abraxane in the treatment of ovarian cancer: The absence of hypersensitivity reactions. *Gynecol Oncol*.
2006;100(2):437-438. doi:10.1016/j.ygyno.2005.09.012

115. Roux KH, Strelets L, Michaelsen TE. Flexibility of human IgG subclasses. *J Immunol*.

1997;159(7):3372 LP - 3382. http://www.jimmunol.org/content/159/7/3372.abstract.

116. Patil Y, Panyam J. Polymeric nanoparticles for siRNA delivery and gene silencing. *Int J*

Pharm. 2009;367(1-2):195-203. doi:10.1016/j.ijpharm.2008.09.039

117. Toti US, Guru BR, Hali M, et al. Targeted delivery of antibiotics to intracellular chlamydial infections using PLGA nanoparticles. *Biomaterials*. 2011;32(27):6606-6613.
doi:10.1016/j.biomaterials.2011.05.038

118. Swaminathan SK, Roger E, Toti U, Niu L, Ohlfest JR, Panyam J. CD133-targeted paclitaxel delivery inhibits local tumor recurrence in a mouse model of breast cancer. *J Control Release*. 2013;171(3):280-287. doi:10.1016/J.JCONREL.2013.07.014

119. Patil YB, Swaminathan SK, Sadhukha T, Ma L, Panyam J. The use of nanoparticlemediated targeted gene silencing and drug delivery to overcome tumor drug resistance. *Biomaterials*. 2010;31(2):358-365. doi:10.1016/J.BIOMATERIALS.2009.09.048

120. Kalscheuer S, Khanna V, Kim H, et al. Discovery of HSPG2 (Perlecan) as a Therapeutic

Target in Triple Negative Breast Cancer. 2019;2(August):1-11. doi:10.1038/s41598-019-

48993-6

121. Murakami M, Cabral H, Matsumoto Y, et al. Improving drug potency and efficacy by nanocarrier-mediated subcellular targeting. *Sci Transl Med*. 2011;3(64). doi:10.1126/scitranslmed.3001385

122. Shen L, Zhang Z, Wang T, Yang X, Huang R, Quan D. Reversed lipid-based nanoparticles dispersed in oil for malignant tumor treatment via intratumoral injection. *Drug Deliv*. 2017;24(1):857-866. doi:10.1080/10717544.2017.1330373

123. Yook S, Cai Z, Lu Y, Winnik MA, Pignol JP, Reilly RM. Intratumorally injected 177Lulabeled gold nanoparticles: Gold nanoseed brachytherapy with application for neoadjuvant treatment of locally advanced breast cancer. *J Nucl Med*. 2016;57(6):936-942. doi:10.2967/jnumed.115.168906

124. Durymanov MO, Rosenkranz AA, Sobolev AS. Current approaches for improving intratumoral accumulation and distribution of nanomedicines. *Theranostics*. 2015;5(9):1007-1020. doi:10.7150/thno.11742

125. Adam Moser, Kevin Range and DMY. 基因的改变 NIH Public Access. *Bone*.

2008;23(1):1-7. doi:10.1038/jid.2014.371

126. NANOPARTICLE-BASED CHEMOTHERAPY. 2015;(August).

127. Makadia HK, Siegel SJ. Poly Lactic-co-Glycolic Acid (PLGA) as Biodegradable

Controlled Drug Delivery Carrier. *Polymers (Basel)*. 2011;3(3):1377-1397.

doi:10.3390/polym3031377

128. Panyam J, Dali MM, Sahoo SK, et al. Polymer degradation and in vitro release of a model protein from poly(D,L-lactide-co-glycolide) nano- and microparticles. *J Control Release*.

2003;92(1-2):173-187. doi:10.1016/s0168-3659(03)00328-6

129. Khanna V, Kalscheuer S, Kirtane A, Zhang W. Perlecan-targeted nanoparticles for drug delivery to triple-negative breast cancer. 2019;1.
130. 2018 NCI Budget Fact Book - Research Funding - National Cancer Institute.

https://www.cancer.gov/about-nci/budget/fact-book/data/research-funding. Accessed December 9, 2019.
131. Siegel RL, Miller KD, Jemal A. Cancer statistics, 2018. *CA Cancer J Clin*. 2018;68(1):7-

30. doi:10.3322/caac.21442

132. Cheng J, Teply BA, Sherifi I, et al. Formulation of functionalized PLGA-PEG nanoparticles for in vivo targeted drug delivery. *Biomaterials*. 2007;28(5):869-876. doi:10.1016/j.biomaterials.2006.09.047
133. Chu X, Wang Y, Meng W, Chen L, Jin M, Chen L. Improving antitumor outcomes for palliative intratumoral injection therapy through lecithin – chitosan nanoparticles loading paclitaxel – cholesterol complex. 2019.